

1 **Linking landslide patterns to transient landscapes in**
2 **the northern Colombian Andes**

3 **Edier Aristizábal^{1,2}, Oliver Korup^{2,3}**

4 ¹Departamento de Geociencias y Medio Ambiente, Universidad Nacional de Colombia, Medellín,

5 Colombia

6 ²Institute of Environmental Science and Geography, University of Potsdam, Germany

7 ³Institute of Geosciences, University of Potsdam, Germany

8 **Key Points:**

- 9
- 10
- 11
- 12
- 13
- 14
- We explore potential links between drainage network dynamics and landslide patterns in the tectonically active Colombian Andes.
 - The distribution of $\sim 14,000$ landslides shows little spatial coincidence with varying channel steepness, though some attraction to actively migrating divides.
 - Clustering of catchment hypsometry instead objectively identifies four progressive stages of catchment transience with differing landslide densities.

15 **Abstract**

16 Landslides are among the most recognizable evidence of hillslope erosion in tectonically
 17 active mountains. Yet, how much of the distribution of landslides of different ages re-
 18 lates to, or inherits from, the pattern of topographic metrics of landscape evolution re-
 19 mains partially unresolved, and especially so in tropical areas. We derive such metrics
 20 for 650 catchments of 10^1 - 10^2 km 2 in size, including their mean hypsometric integral,
 21 local relief, geological lineament density, and stepness variations and knickpoint density
 22 of river channels as proxies of tectonic activity; we test how these proxies match with,
 23 if not explain, the distribution of some 14,000 prehistoric and modern landslides in the
 24 northern Colombian Andes. A K -means cluster analysis of catchment hypsometry re-
 25 veals four distinct groups of catchments. We interpret these groups to reflect different
 26 states of transience with clear contrasts in mean local relief, average hillslope inclination,
 27 channel steepness, and landslide density. We propose that tectonic uplift, base-level changes,
 28 and passing waves of incision control these different states of transience. Yet, we find that
 29 landslides occur widely without much spatial association to, or amassing near, major chan-
 30 nel knickpoints. This observation reflects what we would expect from a threshold land-
 31 scape in which landslides abound irrespective of contrasts in local river incision rates.
 32 Still, we notice a pronounced attraction of landslides to transient divides, where espe-
 33 cially prehistoric landslides are preferentially preserved. In summary, we infer that, in
 34 our study area at least, differences in catchment hypsometry might be more useful to track
 35 potential tectonic controls on landslide patterns than comparing these to knickpoint dis-
 36 tributions or channel metrics.

37 **1 Introduction**

38 Modern views of landscape evolution emphasize the dynamic interaction between
 39 tectonic activity and climatically modulated shifts of mass across the land surface (Davies
 40 et al., 2021; Whittaker, 2012; Alcántara-Ayala, 2002). Tectonic or climate perturbations
 41 may cause transient states, but landscapes move toward an equilibrium in which rock
 42 uplift and denudation are balanced on average (Whittaker, 2012; Wobus et al., 2006; Whipple,
 43 2004). River networks are primary conveyors by which perturbations propagate through
 44 the landscape, and force adjacent hillslopes to respond to changes in base level (Whipple,
 45 2004; Howard, 1994). The geometric configuration of rivers and hillslopes thus encodes
 46 valuable information on tectonic and climatic disturbances (Whipple et al., 2017; Stock
 47 & Montgomery, 1999), offering insights into the dominant geomorphic processes, which
 48 in mountain belts often involve abundant landsliding (Larsen & Montgomery, 2012; Ko-
 49 rup et al., 2010; Montgomery & Brandon, 2002; Campforts et al., 2020; Broeckx et al.,
 50 2020).

51 Several authors emphasize how landslides might control landscape response to catch-
 52 ment perturbations (Montgomery, 2001). Numerical landscape evolution models built
 53 on stream-power models incorporate hillslope-channel coupling and landsliding via mech-
 54 anistic threshold criteria. For example, Egholm et al. (2013) simulated a reciprocal re-
 55 lationship between channel incision and landslides. Their model showed positive feed-
 56 back when landslides increased sediment input and accelerated fluvial incision, whereas
 57 a negative feedback emerged where excess sediment protected the river bed from erosion.
 58 Roering et al. (2015) showed how changes in rock uplift and incision alter the frequency
 59 and pattern of active landslides in the northern California Coastal Ranges. The authors
 60 proposed that areas with greater uplift rates have larger, faster, and more frequent land-
 61 slides. A landscape evolution model by Campforts et al. (2020, 2022) featured stochas-
 62 tic landsliding and its effect on fluvial sediment dynamics and showed that, as rock-uplift
 63 rates increased, so did the frequency and magnitude of landslides, whereas drainage den-
 64 sity and stream concavity decreased.

Despite these studies, the spatial patterns of landsliding remain poorly understood beyond the scope of individual triggers such as earthquakes or rainstorms (Yanites et al., 2018). While susceptibility studies attempt to explain landslide distribution in space, they concentrate on the hillslope scale and use local terrain indices, slope material properties, or land-cover attributes as statistical predictors (Reichenbach et al., 2018; Soeters & Van Westen, 1996; Montgomery & Dietrich, 1994). Yet, how these possible controls play out in terms of entire landslide patterns instead of local, pixel-wise, susceptibility remains uncertain, and thus often described as stochastic (Benda & Dunne, 1997).

A broader view is that landslides form as a local hillslope response to upstream knick-point migration in response to base-level fall into catchments in disequilibrium (Wobus et al., 2006; Hovius & Stark, 2006; Whipple, 2002). Thus, the dynamics of the channel network should control landslide distribution (Montgomery & Dietrich, 1994; Burbank et al., 1996) eventually. Larsen and Montgomery (2012) supported this notion by reporting a significant correlation between landslide frequency, exhumation rates, and stream power in the eastern Himalayas. Tsou et al. (2017) used river and hillslope morphometry to show that transient hillslopes resulting by successive rejuvenated river incisions control the distribution of deep-seated landslides and long-term slope stability in southwestern Japan. Gallen et al. (2011) noted a similar pattern in the southern Appalachians, where local relief is higher, hillslopes steeper, and landslides more abundant in tributary catchments downstream of major knickpoints. The authors used hypsometric analyses to propose a model for determining different evolutionary stages of landscape development. This model posits that the hypsometric distribution of a catchment in equilibrium tends to be skewed toward lower elevations. When a perturbation occurs, it creates a distinct peak in the hypsometric distribution that migrates to higher elevations, moving farther away from a state of equilibrium.

Most of these studies focused on tectonically active mountains in temperate climate zones. In contrast, insights are rare from tropical regions, where rainfall is distinctly seasonal, rates of chemical weathering are high, and the geomorphic legacy of glaciers is minimal. Here, we choose the northern Colombian Andes as an example of a tectonically active and tropical mountain belt dotted by numerous landslides. Landslides are a major natural hazard in Colombia (D. Gómez et al., 2023; Aristizábal & Sánchez, 2020a), though most studies have ignored the potential legacy of tectonic uplift and landscape evolution on where landslides occur. Hence, we examine whether the pattern of prehistoric and recent landslides is linked to metrics of landscape evolution, especially those that help to infer hillslopes and river channel dynamics. In particular, we test the model proposed by Gallen et al. (2011). To this end, we check whether and how well we can objectively derive from digital topographic data different stages of landscape evolution and tectonic activity, and how these help to explain the distribution of widely observed landslides.

2 Study area

The Colombian Andes have unique geomorphic and hydroclimatological characteristics that result from their tectonic and equatorial setting (Fig. 1). In the northern Andes, geological features are controlled by the diagonal convergence of the Nazca and Caribbean oceanic plates with the South American continental plate (Cediel et al., 2003; Acosta et al., 2007; Trenkamp et al., 2002). This transpressional accretion features two distinct crustal blocks: the Northern Andean Block (NAB) is moving in a north-westward direction, whereas the Panamá-Chocó Block (PCB) is moving in a south-eastward direction, in relation to the South American Plate (Kellogg et al., 1995). The accretion of the PCB caused the Nazca Plate to rupture at about 5°N, causing flat slab subduction in the north (Taboada et al., 2000). In contrast, the south has a steeper subduction angle and active volcanoes (Pérez-Consuegra et al., 2021; Restrepo-Moreno et al., 2019; Farris et al., 2011; Taboada et al., 2000; Mann & Corrigan, 1990) (Fig. 1).

Our study area is located in the Colombian Andes north of 5°N, and covers the Western Cordillera (WC) and relic high-elevation (~2500 m a.s.l.), low-relief, and flat-topped erosional surfaces of the Central Cordillera (CC), known as the Antioqueño Plateau (AP) that is deeply incised by the Nechí River, the main tributary of the Cauca River. The study area features the Cauca canyon (Fig. 2A), and is bounded by broad alluvial flats to the west of the Atrató River, to the east by the Magdalena River, and to the north by the Cauca River.

The study area covers some 48.000 km², which we divided into 650 catchments of similar areas and stream orders. About 75% of these catchments drain less than 100 km² each, with a median area of 36 km². The catchments have average slopes between 15° and 25° with a relief ranging from 180 m to 380 m, and up to 750 m in the northern Cauca canyon (Fig. 3). Narrow valleys bounded by steep slopes characterize the WC and eastern flanks of the CC. The area is composed of several geological terranes that have attached to South America since the Cretaceous (Cediel et al., 2003). The eastern terranes of Cauca-Romeral Fault System (CRFS) have intrusive Mesozoic rocks on a Precambrian basement of continental rocks and Cenozoic volcanic activity (Cediel et al., 2003), while the western terranes are made up of collided oceanic blocks and (ultra-)mafic island arcs that formed in the Late Cretaceous (Cardona et al., 2012).

The PCB is colliding with the NAB at 15–18 mm/yr, producing rapid deformation in the northern Colombian Andes (Kellogg et al., 2019) and reactivating tectonic structures into oblique left-lateral normal faults and right-lateral faults (Acosta et al., 2007). For the study area, Pérez-Consuegra et al. (2021, 2022) proposed that the collision of the PCB and slab flattening in the northern Nazca subduction zone caused increased surface uplift that is highest in the western and central parts of the northern CC, and markedly lower in the east. Restrepo-Moreno et al. (2019) and Noriega-Londoño et al. (2020) inferred pulses of exhumation during the Paleocene–Eocene and Oligocene–Miocene, at rates of 0.2–0.9 km/Ma, separated by phases of low exhumation rates (<0.02 km/Ma) that may have favoured the development of the AP. Exhumation rates of the Eastern Cordillera have been at 1–1.5 mm/yr since 3 Ma (Mora et al., 2010). For the CC, Arboleda et al. (2015) reported rates of 1.5 km/Ma between 11 Ma and 6 Ma, while Ott et al. (2023) proposed that Late Miocene slab flattening accelerated surface uplift (~2 km) in the northern Colombian Andes, maintaining landscape disequilibrium to the present day.

Generally north trending geological structures dominate the northern Colombian Andes (Fig. 2B), especially the left-lateral Cauca-Romeral Fault System (CRFS) that separates oceanic rocks to the west from continental rocks to the east (Egholm et al., 2013; Ego et al., 1995). The Itsmina Deformation Zone (IDZ), The Espíritu Santo Fault (ESF), and Palestina Fault System (PFS) are major NE-trending fault systems. The PFS is a right-lateral strike-slip structure with NW-SE antithetic faults in the intrusive rock of the CC (Acosta et al., 2007; Feininger, 1970). The ESF is a right-lateral oblique strike-slip fault with normal components in the northeast and reverse components in the southwest (Noriega-Londoño et al., 2020; Page, 1986). The IDZ marks the southern border of the PCB, and is characterized by transpressive right-lateral faults (Acosta et al., 2007; Taboada et al., 2000). Lastly, the Uramita Fault system (UFS) and Arma Fault (AF) are among the NW-trending faults. While the AF is oblique normal, left-lateral, the UFS is a N-NW striking conjugate structure marking the eastern boundary of the PCB with transpressive left-lateral motion (Acosta et al., 2007; Taboada et al., 2000).

Both the high-relief landscape of the WC and the low-relief terrain of the CC feature thick weathering profiles with saprolitic and residual soils. On the granitoids, weathering profiles consist of deep yellowish-red (Munsell 10YR 7/4) residual soils and saprolites over 50-m thick overlying up to 100 m of chemically disintegrated rock (Aristizábal et al., 2005). Weathering profiles developed on ultra-basic and metamorphic rocks are thinner, mostly reddish orange (7.5YR 7/6), and contain highly weathered rock fragments (Aristizábal et al., 2005).

Precipitation in the Colombian Andes has a bimodal annual cycle driven by the passage of the intertropical convergence zone (ITCZ) (Bedoya-Soto et al., 2019). This seasonal pattern is modulated by the topographic gradients of the Andes that favour deep convection and trigger local intensive storms (Poveda et al., 2011). The mean annual precipitation ranges from 1,000-8,000 mm, but the distribution of rainfall varies locally: the more humid western range front receives extreme totals of between 8,000-13,000 mm (Poveda & Mesa, 2000; Smith, 2006), whereas the Cauca canyon in the center of our study area canyon receives some 1,000 mm (Fig. 3). Partly mirroring this precipitation gradient, dense forest covers most of the WC terrains and the eastern flank of the CC, whereas grass dominates on highlands of the AP and on the Magdalena River lowlands. Rainfall and topographical swath profiles highlight the strong influence of the Andes terrains on rainfall (Fig. 9).

The study area is prone to landslides (Aristizábal & Sánchez, 2020b; D. Gómez et al., 2023), some of which have led to significant loss of life and substantial economic impacts. Most historic slope failures initiated along contacts of residual soils and the saprolite as shallow translational slides that, in many cases, transformed into debris flows. Several of these shallow landslides formed entire clusters in the higher elevations of the CC and WC, where forest cover is dense. In contrast, recent larger and deep-seated landslides with multiple retrogressive and successive rotational slides have been reported along narrow and low-order streams.

Documented landslides are biased toward urban areas, as historical or media reports tend to focus on landslides causing damage in populated areas (Guzzetti et al., 2012; Froude & Petley, 2018). More general information about landslides comes from optical remote sensing, which is compromised by frequent cloud in the northern and western fringes of our study area especially. Rainfall has triggered 92% of all landslides reported in the Colombian Andes between 1970 and 2023, while strong earthquakes or active volcanism were absent during this period (Aristizábal & Sánchez, 2020a). The triggers of the older, prehistoric landslides generally remain unknown, but strong seismic ground shaking is a likely mechanism for generating even larger slope failures than those reported in past decades. Many catchments host evidence of large scars and deposits of older landslides that have eluded any systematic documentation so far.

3 Data and Methods

From the viewpoint of inferring process from form, various morphometric methods, such as hypsometric analysis (Strahler, 1952) or river longitudinal profiles (Wobus et al., 2006), have been popular for measuring topography as the time-integrated result of coupled tectonics, climate and erosion (Whittaker, 2012; Perron & Royden, 2013; Willett et al., 2014). We used two digital elevation models (DEMs) for both terrain analysis and landslide mapping, drawing on data from the Shuttle Radar Topography Mission (SRTM) at 30 m (Farr et al., 2007), and the Advanced Land Observing Satellite-Phased Array-Type L-Band Synthetic Aperture Radar (ALOS-PALSAR) at 12.5 m (Logan et al., 2014).

We compiled two catalogues of landslides based on their approximate timing: we mapped recent landslides that occurred between 1970 and 2023 (Fig. 4) from high-resolution (<1 m) optical satellite images in Google Earth™. Apart from contrasts in color and terrain, we used fresh scars of bare rock or soil as a key diagnostic of landsliding. We separately mapped prehistoric landslides that are mainly deep-seated and that eluded historic landslide databases or optical satellite imagery, but remain well preserved or large enough to stand out in hillshaded SRTM and ALOS-PALSAR DEMs as distinct areas of subdued terrain with differing hillslope inclination, roughness, and local drainage density. All of thus discovered prehistoric landslides have clearly defined head scarps and bodies (Fig. 4).

To estimate the influence of the tectonic history on landslide occurrence, we extracted the density of geological lineaments using the LINE algorithms of the image processing and optimization software CATALYST on the SRTM data, based on eight hillshade directions with 45°-bins of azimuth, at a sun elevation of 45°. Given the size of the study area, we only considered lineaments >1 km. We used the Climate Hazard Group InfraRed Precipitation with Station Data (CHIRPS) (Funk et al., 2015), version 2.0, to obtain rainfall data at 5-km resolution from 1981 to 2023.

We derived river longitudinal profiles and local slope and elevation data with QGIS. To detect knickpoints, we used TopoToolbox's KnickpointFinder function (Schwanghart & Scherler, 2014), which iteratively adjusts river profiles to a strictly concave upward shape with a tolerance value that we set to 100 m using the 12.5-m DEM. We estimated local relief as the maximum elevation difference in a 1-km radius using the SRTM DEM in Google Earth Engine (Moore & Hansen, 2011). We computed the hypsometric integral HI for the 650 catchments in the study area using WhiteToolBox (Lindsay, 2014) and the ALOS-PALSAR data; HI is a measure of the "volume" of the catchment bounded by its divides, and has been used as proxy for stages in landscape development (Strahler, 1952; Gallen et al., 2011). To identify objectively these stages, we tested several clustering methods to group catchment-wide hypsometry into similar classes. To this end, we used normalized and binned elevation data for each catchment. We considered K -means clustering with a Euclidean distance; time series K -means with a Dynamic Time Warping (DTW) and a soft DTW metric; and Agglomerative Clustering with a connectivity matrix using different K -nearest neighbours for $K = 1, 2, 4$, and 10. To this end, we used the Python Scikit-Learn library (Pedregosa et al., 2011). We used the elbow method to estimate the optimal number of clusters by plotting the within-cluster sum of squares (WCSS) as a function of K to identify the break point where the rate of decrease in WCSS changes most (Thorndike, 1953). We also used the Silhouette coefficient (S_c) to measure how similar a catchment is to its own cluster (cohesion) versus other clusters (separation), and ranges from -1 (not clustered) to +1 (clustered) (Rousseeuw, 1987).

We estimated the χ coordinate values using the equation 3 proposed by Perron and Royden (2013). They integrate Eq. 3 along the channel longitudinal coordinate x from a reference point x_b . We used the confluence of the Cauca and Magdalena Rivers as base level; for the western drainage network, the base level was set by the Atrató River. This approach transforms the horizontal coordinates of the river profile into a variable χ that accounts for longitudinal variations in the drainage area (A) (Mudd et al., 2014).

$$z(x) = z(x_b) + \left(\frac{U}{KA_0^m} \right)^{1/n} \int_{x_b}^x \frac{A_0}{A(x)}^{m/n} \partial x \quad \text{or} \quad z(x) = z(x_b) + k_{sn}\chi, \quad (1)$$

where k_{sn} is the local channel steepness conformed by the uplift (U) and the erosion (E) rates, and it is corrected for a reference drainage area ($A_0 = 1 \text{ km}^2$) to normalize river profiles (Whipple et al., 2017). whilst, m and n are empirically derived coefficients as parts of the channel concavity index ($\theta = m/n$), we used $\theta = 0.45$ (Wobus et al., 2006). Willett et al. (2014) proposed using χ -maps to interpret the dynamics and relative stability of drainage divides. Steady-state catchments should have equal χ values across shared divides, whereas transient states are inferred from differing χ values, with divides migrating in the direction of larger χ (Willett et al., 2014). We implemented LSDTopoTools (Mudd et al., 2014) and TopoToolbox (Schwanghart & Scherler, 2014) using the SRTM dataset.

266 **4 Results**

267 **4.1 Landslides and the drainage network**

268 We detected 13,777 recent landslides and 222 prehistoric landslides (Fig. 4) throughout
 269 the Cauca canyon, the northern Atrató basin, and the southeastern Magdalena basin.
 270 Landslides are most abundant in the Cauca basin with an average density of $0.25/\text{km}^2$,
 271 followed by the Atrató basin ($0.22/\text{km}^2$), and the Magdalena ($0.18/\text{km}^2$). We checked
 272 whether and how large knickpoints in the channel network, defined here as having a vertical
 273 height >100 m, affect the distribution of landslides. We expect that landslides are
 274 more abundant below active knickpoints, reflecting the response of steepened hillslopes
 275 to passing waves of river incision. The 558 large knickpoints that we identified in the study
 276 area and its three major basins, i.e. the Atrató, Cauca, and Magdalena (Fig. 5), fail to
 277 show a clear, overarching spatial coincidence with the mapped slope failures: for the western
 278 study area, we find that landslides abound even without any major knickpoints present.
 279 In the Atrató basin, we find that recent landslides are largely located higher than major
 280 knickpoints, whereas landslides in the Cauca are mainly below. The pattern is less
 281 conclusive for the Magdalena basin.

282 To identify transient catchments we compared river profiles in χ -space (Fig. 10).
 283 Similar values on both sides of divides suggest the two opposite drainage are at equilibrium,
 284 whereas high contrasts in χ values imply stream piracy leading to divide migration. We observed competing divides marked by high contrasts in χ values (Fig. 10) that
 285 abound in the Cauca River, which captures catchments toward the west and east (T1).
 286 We also detected a strong contrast in the northeastern study area, mainly tied to the Nechí²⁸⁷
 287 River that undermines catchments to the northwest and southeast (T2); tributaries of
 288 the Nechí River have divides that tend to migrate to the northeast (T3). In the Mag-
 289 dalena basin, divides seem to move to the southeast (T4). How far away landslides oc-
 290 cur with respect to the nearest active divides differs markedly between prehistoric and
 291 recent failures: the latter are large distributed randomly within 25 km, whereas prehis-
 292 toric landslides tend to cluster nearer to transient divides (Fig. 10c, d).

294 **4.2 Landslides and catchment hypsometry**

295 We find that catchments with mapped landslides have a distinctly higher HI than
 296 those without (Fig. 6A). Catchments with prehistoric landslides tend to have higher HI
 297 values than those hosting recent landslides (Fig. 6A). Catchments with landslides also
 298 have a higher mean local relief of $330 \text{ m} \pm 132 \text{ m}$ compared to $185 \text{ m} \pm 134 \text{ m}$ in catchments
 299 without, and tend to be steeper with average slopes of $21^\circ \pm 6^\circ$, compared to $14^\circ \pm 7^\circ$. We
 300 find that, in the Cauca and Atrató basins, HI is negatively correlated with mean annual
 301 rainfall (Fig. 6A). For the wetter portions in the western Atrató basin this negative cor-
 302 relations is strongest, but levels out in the drier, eastern Magdalena basin.

303 To learn whether and how catchment hypsometry (as a proxy of landscape tran-
 304 sience) differs between the 650 catchments, we ran cluster analyses on their binned and
 305 normalized elevation distributions (Fig. 7). We find that four clusters is the optimal num-
 306 ber for both K -means clustering with an Euclidean distance, and as time series K -means
 307 clustering with the softDTW metric. We observe that these four hypsometric clusters
 308 have distinct peaks at differing normalized elevations: cluster A has a hypsometric dis-
 309 tribution skewed to lower elevations; cluster C has a more symmetric hypsometry, while
 310 cluster D is skewed to higher elevations. Cluster A catchments are mainly in the west-
 311 ern, eastern, and northern study area, and along the high-elevation, low-relief surfaces
 312 of the Cauca and Magdalena basins (Fig. 7A). Cluster B catchments dominate the west-
 313 ern flank of the Cauca Canyon, whereas cluster D catchments sit mostly along its east-
 314 ern flank. Finally, cluster C drains mostly the western flanks of the northern Cauca River,
 315 and its eastern flanks further south.

The four clusters have different distributions of catchment-wide *HI*, local relief, slope, k_{sn} , landslide density, and mean annual rainfall (Fig. 8), though no distinct grouping or alignment with respect to major rock types. Mean *HI* increases for catchments from cluster A to cluster D, and so do mean local relief, mean slope, mean k_{sn} , landslide density, except for cluster D, where these metrics are among the second lowest overall (Fig. 8). About half (53%) of the prehistoric landslides are in catchments of cluster C, followed by clusters D (22%) and B (16%). In contrast, 74% of recent landslides occur in clusters B (36%) and C (38%). Major knickpoints mainly concentrate in clusters D (39%) and C (32%), followed by clusters B (19%) and A (10%). Recent landslides failed close to the normalised elevation peaks, whilst prehistoric landslides in cluster A and D dominate higher relative elevations. Catchments of cluster A tend to have high channel concavities with low relative elevations (Fig. 9), while cluster B and C have less concave channels; catchments of Cluster D have more convex channel profiles.

5 Discussion

5.1 Hypsometric clustering and transient catchments

The northern Colombian Andes combine steep mountains and plateaus in an active tectonic setting with pronounced landslide activity. Objective clustering of hypsometric data highlights four distinct groups of catchments with peaks at different relative elevations. Following Gallen et al. (2011), we interpret these four groups as progressive stages of an evolving drainage network. Given the variation in catchment mean slope, mean relief, hypsometric distribution, channel concavity, and landslide abundance, we surmise that the clusters represent different stages of landscape evolution in terms of departure from topographic equilibrium (Fig. 8). Normalized elevation peaks are lowest in cluster A, and highest in cluster D (Fig. 7A). We argue that the distribution of these dominant elevations shifts up in response to tectonic uplift until fully recovering a state of balanced uplift and erosion with mostly low relative elevations (Gallen et al., 2011). Catchments in cluster A thus most likely reflect this topographic equilibrium. Increases in uplift rates prompt channels to incise commensurately, thus changing hypsometric distributions by increasing the proportion of higher elevations (Cluster B, C, and D), until channels and hilltops have adjusted to the new base level (Fig. 7). Steep channels with high values of  and contrasting χ -values across drainage divides support the idea that many catchments with numerous landslides are in transient states (Fig. 10).

Most of these transient catchments are close to geological lineaments and active fault systems (Fig. 2), such as the margins of the Cordilleras and the Antioqueño Plateau where catchments of cluster A prevail. Hypsometric clusters B and C indicate transience along the Palestina Fault (PF) and west of the Cauca-Romeral Fault System (CRFS), whereas cluster D points at topographic equilibrium on the northeastern side (Fig. 7). This might be a consequence of tectonic uplift of the western block or at least higher rates to the west (Pérez-Consuegra et al., 2021) and lower rates to the  east. Our results show that the southeastern catchments are moving away from an  equilibrium state, probably associated with recent activation of the PF (Acosta et al., 2007; Feininger, 1970). This interpretation is consistent with four dominant trends that we identify the inferred migration of transient catchment divides: two trends are normal to the Cauca canyon (T1) and the Nechí catchment (T2), while two others have a northeastern (T3) and south-eastern (T4) direction in the eastern Central Cordillera (CC). The Cauca trend (T1) and trend T2 are consistent with a northeast-ward tectonic tilting; trend T2 supports the idea by Arias (1995), who argued that the Nechí River is capturing the Grande and Aburrá Rivers that had drained to the Magdalena River earlier.

Previous thermochronometric and morphometric studies reported accelerated surface uplift in the northern Colombian Andes since Pliocene times (Restrepo-Moreno et al., 2019; Noriega-Londoño et al., 2020; Pérez-Consuegra et al., 2021, 2022; Ott et al.,

367). The collision of the Panamá-Chocó Block (PCB) and the beginning of slab flattening caused surface uplift over the past 6-7 Myr, with faster tectonic uplift to the west (Pérez-Consuegra et al., 2021; Ott et al., 2023), creating up to 3 km of relief in the Cauca Canyon. The resulting wave of erosion would have moved upstream along the Nechí River and its tributaries, forming multiple knickpoints. Our morphometric analyses support the notion of higher recent uplift rates to the west (Fig. 10). Hillslopes tend to become less steep toward the northeast on average, and there is a marked trend of river capture to the northeast of the Nechí River, such as the capture of the paleo-Grande and paleo-Aburrá Rivers by the Nechí River. More catchments appear to be returning to equilibrium state in cluster D than in clusters B and C in the northeast. The catchments along the PFS show a similar trend; transient catchments moving away from a state of equilibrium (clusters B and C) are prolific in the SW, consistent with the idea of a tilt to the northeast.

380 Apart from supporting previous findings about recent accelerated and spatially varying
 381 tectonic uplift of our study area, our findings also lend support to the model proposed
 382 by Gallen et al. (2011). Our results indicate a link between catchment hypsometry and
 383 landscape transience, given the diverse differences in hillslope and channel steepness across
 384 the four clusters. Local base-level drops and knickpoint migration in small catchments
 385 have been reported in the Cauca basin and the Nechí catchment (Pérez-Consuegra et
 386 al., 2021; Aristizábal & Yokota, 2008; Noriega-Londoño et al., 2020). We interpret that
 387 the major knickpoints at least are the result of recent tectonic uplift pulses associated
 388 with the collision of the Panamá-Chocó Block (PCB) and flattening of slab subduction
 389 (Ott et al., 2023).

390 5.2 Distribution of landslides

391 We find that landslides in the northern Colombian Andes occur mainly in catchments with high HI , though rarely in the wettest part of the landscape, where their geomorphic evidence may be censored by dense vegetation or triggers that are rare and poorly captured by our inventory (Fig. 6). This masking effect may also explain the vertical concentration of landslides above major knickpoints in the Atrató basin, where much steeper channel sections downstream seem to be curiously devoid of slope failures (Fig. 5). In most of the remaining study area, however, landslides are more densely concentrated in transient catchments, and least abundant in catchments of cluster A, which is nearest to topographic equilibrium (Figs. 8). Our results support the notion that catchment hypsometry can help to evaluate the current and future state of hillslope stability (Gallen et al., 2011), at least in our study area.

402 In this context, we stress the negative correlation between mean annual rainfall and
 403 HI ; this correlation is strongest in the Atrató basin, where annual rainfall totals are high,
 404 dense forest cover, landslide density is high while knickpoints density is low. In contrast, the Magdalena basin has the lowest values mean annual rainfall with next to no
 405 correlation with HI , as well as low landslide density and high knickpoint density. We sur-
 406 mise that our hypsometric clustering thus likely contains effects of rainfall and hence,
 407 to some degree, the hydrological causes and triggers of landslides. Rainfall in the north-
 408 ern Colombian Andes varies strongly even across short (km-scale) distances. (Montgomery
 409 et al., 2001) explored hypsometric curves to analyze the influence of zonal climate regimes
 410 on the orogen-scale morphology of the Andes, and found consistent patterns with vari-
 411 ations in erosional processes. They observed concave-up hypsometric curves in the north-
 412 ern Andes, reflecting the dominance of river erosion in a wet tropical climate. In con-
 413 trast, hypsometric curves in the Central Andes are nearly linear and thought to repre-
 414 sent mainly the effects tectonic uplift; finally, hypsometric curves in the southern An-
 415 des show a shoulder that may reflect effects of glaciation (Montgomery et al., 2001).

417 While both changes in hypsometric distributions and knickpoints have been linked
 418 to imbalanced rates of erosion and tectonic uplift (Pérez-Peña et al., 2009), we find lit-
 419 ttle correspondence between the distributions of landslides and major knickpoints for the
 420 entire study area (Fig. 7). This observation might indicate a threshold landscape, in which
 421 hillslopes are steep enough that landslides occur widely and without relation to contrasts
 422 in local channel incision rates. Some knickpoints may also be unrelated to tectonic ac-
 423 tivity and instead mark lithological contrasts or the effects of natural dams. Contrast-
 424 ing patterns emerge for individual major basins, however. In the Atrató basin, recent
 425 landslides lie higher than knickpoints and are farther from the basin outlets, even if ac-
 426 counting for local hillslope length. The opposite is the case in the Cauca basin, where
 427 landslides mostly occur below major knickpoints and thus consistent with the model of
 428 delayed hillslopes adjusting via mass wasting to passing waves of fluvial incision. Despite
 429 the lack of any clear pattern of landslides and major knickpoints, we observe that land-
 430 slides occur mainly within 25 km of migrating drainage divides. In particular, the den-
 431 sity of larger, prehistoric landslides is highest close (<10 km) to these divides. In con-
 432 trast, the distribution of recent landslides with respect to these divides hardly differs from
 433 a random pattern (Fig. 10). While this difference may arise from sample sizes that dif-
 434 fer by two orders of magnitude between recent and prehistoric landslides, we recall that
 435 models of stochastic landsliding and associated sediment dynamics (Campforts et al., 2020,
 436 2022) observed that, if the rate of uplift exceeds that of vertical weathering, landslides
 437 can concentrate near ridges. At least for larger landslides deposits, these locations would
 438 be more preferable for longer preservation and hence detection from digital elevation mod-
 439 els.

440 6 Conclusions

441 Studies that relate landslide occurrence to metrics of landscape evolution have been
 442 rare in tropical settings, and especially so in the northern Colombian Andes. There, land-
 443 slide studies have largely adopted the strategy of estimating susceptibility at the scale
 444 of individual hillslopes or pixels without much regarding of tectonic uplift, river incision,
 445 and landscape adjustments that operate on geological timescales. To meet this short-
 446 coming, we investigated the spatial distribution of some 14,000 landslides with respect
 447 to several morphometric parameters that characterise the dynamics of the drainage net-
 448 work and hillslopes, and the hypsometry of 650 small- to moderate-sized mountain catch-
 449 ments.

450 We find that comparing the distribution of landslides to that of major knickpoints
 451 offers contrasting patterns, though only when looking at large, individual drainage basins.
 452 In several parts of our study, landslides abound without a clear connection to metrics
 453 of channel dynamics. This supports the idea of a threshold landscape in which lands-
 454 liding occurs frequently and widely, and without much correlation to knickpoint loca-
 455 tions and commensurate variations in channel incision rates.

456 In contrast, a cluster analysis of catchment hypsometry reveals four distinct groups
 457 of landscape transience with marked differences in both hillslope and channel steepness
 458 and landslide density. We find that, with this method, the potential role of tectonically
 459 driven long-term landscape evolution on landslide occurrence is more tangible. Catch-
 460 ments with higher tectonic uplift rates exhibit higher levels of landscape disequilibrium,
 461 characterized by steep slopes, high local relief, high HI and K_{sn} values, and a higher den-
 462 sity of landslides, which are prolific close to transient divides, especially prehistoric ones.
 463 Recent landslides tend to occur in catchments experiencing active uplift and rejuvena-
 464 tion, while prehistoric landslides are more prevalent in catchments closer to equilibrium.

465 Our study highlights the relevance of catchment rejuvenation and drainage reor-
 466 ganization in shaping landscape morphology and influencing landslide distribution. Yet,
 467 we also learn that not all methods or metrics might work equally well to show this con-

468
469
470
471
nection. Transient catchment divides play a crucial role in transferring landscape per-
turbations and triggering landslides. Understanding the interplay between geomorphic
processes, landscape evolution, and natural hazards may aid sustainable risk manage-
ment and land-use planning.

472
473
474
475
Our findings might have novel implications for landslide susceptibility analyses. Al-
though landsliding is a local phenomenon at the hillslope scale, we argue that landscape
evolution drives landslide susceptibility in the long term. Hence, this susceptibility may
be dynamically controlled by the progressive transient stages in a given catchment.

476 7 Open Research

477 Data and code used for this study are fully available in Github ([https://github
.com/edieraristizabal/PAPER_LandscapeEvolutionn](https://github.com/edieraristizabal/PAPER_LandscapeEvolutionn)).

479 Acknowledgments

480 We gratefully acknowledge the support of the Alexander von Humboldt Foundation for
481 awarding the first author a Georg Forster Research Fellowship for Experienced Researchers.
482 This fellowship has been instrumental in facilitating our research endeavors and has pro-
483 vided invaluable opportunities for collaboration and academic growth.

484 References

- 485 Acosta, J., Velandia, F., Osorio, J., Lonergan, L., & Mora, H. (2007). Strike-slip
486 deformation within the colombian andes. *Geological Society, London, Special
487 Publications*, 272(1), 303–319.
- 488 Alcántara-Ayala, I. (2002). Geomorphology, natural hazards, vulnerability and pre-
489 ventionof natural disasters in developing countries. *Geomorphology*, 47, 107-
490 124.
- 491 Arboleda, M., Ceron, M. I. M., & Bermudez, M. (2015). Miocene-pliocene exhumation
492 in the middle cauca belt, colombia. *MSc thesis*, 1-141.
- 493 Arias, L. A. (1995). El relieve de la zona dental de antioquia: un palimpsesto de
494 eventos tectónicos y climáticos. *Centro de Investigaciones Ambientales, Uni-
495 versidad de Antioquia, in spanish*(10), 9-24.
- 496 Aristizábal, E., Roser, B., & Yokota, S. (2005). Tropical chemical weathering of
497 hillslope deposits and bedrock source in the aburrá valley, northern colombian
498 andes. *Engineering Geology*, 81(4), 389–406.
- 499 Aristizábal, E., & Sánchez, O. (2020a). Spatial and temporal patterns and the so-
500 cioeconomic impacts of landslides in the tropical and mountainous colombian
501 andes. *Disasters*, 44(3), 596–618.
- 502 Aristizábal, E., & Sánchez, O. (2020b). Spatial and temporal patterns and the so-
503 cioeconomic impacts of landslides in the tropical and mountainous colombian
504 andes. *Disasters*, 44(3), 596–618.
- 505 Aristizábal, E., & Yokota, S. (2008). Evolución geomorfológica del valle de aburrá
506 y sus implicaciones en la ocurrencia de movimientos en masa. *Boletín de Cien-
507 cias de la Tierra*(24), 05–18.
- 508 Bedoya-Soto, J. M., Aristizábal, E., Carmona, A. M., & Poveda, G. (2019). Sea-
509 sonal shift of the diurnal cycle of rainfall over medellin's valley, central andes
510 of colombia (1998–2005). *Frontiers in Earth Science*, 7, 92.
- 511 Benda, L., & Dunne, T. (1997). Stochastic forcing of sediment supply to chan-
512 nel networks from landsliding and debris flow. *Water Resources Research*, 33,
513 2849-2863. doi: 10.1029/97WR02388
- 514 Broeckx, J., Rossi, M., Lijnen, K., Campforts, B., Poesen, J., & Vanmaercke, M.
515 (2020, 2). Landslide mobilization rates: A global analysis and model. *Earth-*

- Science Reviews, 201. doi: 10.1016/j.earscirev.2019.102972

Burbank, D. W., Leland, J., Fielding, E., Anderson, R. S., Brozovic, N., Reid, M. R., & Duncan, C. (1996). Bedrock incision, rock uplift and threshold hillslopes in the northwestern himalayas. *Nature*, 379(6565), 505–510.

Campforts, B., Shobe, C. M., Overeem, I., & Tucker, G. E. (2022, 8). The art of landslides: How stochastic mass wasting shapes topography and influences landscape dynamics. *Journal of Geophysical Research: Earth Surface*, 127. Retrieved from <https://onlinelibrary.wiley.com/doi/10.1029/2022JF006745> doi: 10.1029/2022JF006745

Campforts, B., Shobe, C. M., Steer, P., Vanmaercke, M., & Lague, D. (2020). Hy-lands 1 . 0 : a hybrid landscape evolution model to simulate the impact of landslides and landslide-derived sediment on landscape evolution. , 3863-3886.

Cardona, A., Montes, C., Ayala, C., Bustamante, C., Hoyos, N., Montenegro, O., ... others (2012). From arc-continent collision to continuous convergence, clues from paleogene conglomerates along the southern caribbean–south america plate boundary. *Tectonophysics*, 580, 58–87.

Cediel, F., Shaw, R. P., & Cceres, C. (2003). Tectonic assembly of the northern andean block. *AAPG Special Volumes*.

Davies, T. R., Korup, O., & Clague, J. J. (2021). Geomorphology and natural hazards: Understanding landscape change for disaster mitigation. *American Geophysical Union*, 576.

Egholm, D. L., Knudsen, M. F., & Sandiford, M. (2013). Lifespan of mountain ranges scaled by feedbacks between landsliding and erosion by rivers. *Nature*, 498, 475-478. doi: 10.1038/nature12218

Ego, F., Sébrier, M., & Yépez, H. (1995). Is the cauca-patia and romeral fault system left or rightlateral? *Geophysical Research Letters*, 22(1), 33–36.

Farr, T. G., Rosen, P. A., Caro, E., Crippen, R., Duren, R., Hensley, S., ... others (2007). The shuttle radar topography mission. *Reviews of geophysics*, 45(2).

Farris, D. W., Jaramillo, C., Bayona, G., Restrepo-Moreno, S. A., Montes, C., Cardona, A., ... Valencia, V. (2011). Fracturing of the panamanian isthmus during initial collision with south america. *Geology*, 39(11), 1007–1010.

Feininger, T. (1970). The palestina fault, colombia. *Geological Society of America Bulletin*, 81(4), 1201–1216.

Froude, M. J., & Petley, D. N. (2018). Global fatal landslide occurrence from 2004 to 2016. *Natural Hazards and Earth System Sciences*, 18(8), 2161–2181.

Funk, C., Peterson, P., Landsfeld, M., Pedreros, D., Verdin, J., Shukla, S., ... others (2015). The climate hazards infrared precipitation with stations—a new environmental record for monitoring extremes. *Scientific data*, 2(1), 1–21.

Gallen, S. F., Wegmann, K. W., Franke, K. L., Hughes, S., Lewis, R. Q., Lyons, N., ... Witt, A. C. (2011, 7). Hillslope response to knickpoint migration in the southern appalachians: Implications for the evolution of post-orogenic landscapes. *Earth Surface Processes and Landforms*, 36, 1254-1267. doi: 10.1002/esp.2150

Gómez, D., García, E. F., & Aristizábal, E. (2023). Spatial and temporal landslide distributions using global and open landslide databases. *Natural Hazards*, 117(1), 25–55.

Gómez, J., Nivia, Á., Montes, N., Diederix, H., Almanza, M., Alcárcel, F., & Madrid, C. (2015). Explanatory notes: Geological map of colombia. *Com- pilando la geología de Colombia: Una visión a*, 35–60.

Guzzetti, F., Mondini, A. C., Cardinali, M., Fiorucci, F., Santangelo, M., & Chang, K.-T. (2012). Landslide inventory maps: New tools for an old problem. *Earth- Science Reviews*, 112(1-2), 42–66.

Hovius, N., & Stark, C. (2006). Landslide-driven erosion and topographic evolution of active mountain belts. In *Landslides from massive rock slope failure* (pp. 573–590).

- Howard, A. D. (1994). A detachment-limited model of drainage basin evolution. *Water resources research*, 30(7), 2261–2285.
- Kellogg, J. N., Camelio, G. B. F., & Mora-Páez, H. (2019). Cenozoic tectonic evolution of the north andes with constraints from volcanic ages, seismic reflection, and satellite geodesy. In *Andean tectonics* (pp. 69–102). Elsevier.
- Kellogg, J. N., Vega, V., Stallings, T., & Aiken, C. L. (1995). Tectonic development of panama, costa rica, and the colombian andes: constraints from global positioning system geodetic studies and gravity. *Special Papers-Geological Society of America*, 75–75.
- Korup, O., Densmore, A. L., & Schlunegger, F. (2010). The role of landslides in mountain range evolution. *Geomorphology*, 120(1-2), 77–90.
- Larsen, I. J., & Montgomery, D. R. (2012, 7). Landslide erosion coupled to tectonics and river incision. *Nature Geoscience*, 5, 468-473. doi: 10.1038/ngeo1479
- Lindsay, J. (2014). The whitebox geospatial analysis tools project and open-access gis. *Proceedings of the GIS Research UK 22nd Annual Conference*. doi: 10.13140/RG.2.1.1010.8962
- Logan, T. A., Nicoll, J., Laurencelle, J., Hogenson, K., Gens, R., Buechler, B., ... others (2014). Radiometrically terrain corrected alos palsar data available from the alaska satellite facility. In *Agu fall meeting abstracts* (Vol. 2014, pp. IN33B-3762).
- Mann, P., & Corrigan, J. (1990). Model for late neogene deformation in panama. *Geology*, 18(6), 558–562.
- Montgomery, D. R. (2001). Slope distributions, threshold hillslopes, and steady-state topography. *American Journal of science*, 301(4-5), 432–454.
- Montgomery, D. R., Balco, G., & Willett, S. D. (2001). Climate, tectonics, and the morphology of the andes. *Geology*, 29(7), 579–582.
- Montgomery, D. R., & Brandon, M. T. (2002). Topographic controls on erosion rates in tectonically active mountain ranges. *Earth and Planetary Science Letters*, 201, 481-489. doi: 10.1016/S0012-821X(02)00725-2
- Montgomery, D. R., & Dietrich, W. E. (1994). A physically based model for the topographic control on shallow landsliding. *Water resources research*, 30(4), 1153–1171.
- Moore, R., & Hansen, M. (2011). Google earth engine: a new cloud-computing platform for global-scale earth observation data and analysis. In *Agu fall meeting abstracts* (Vol. 2011, pp. IN43C-02).
- Mora, A., Horton, B. K., Mesa, A., Rubiano, J., Ketcham, R. A., Parra, M., ... Stockli, D. F. (2010). Migration of cenozoic deformation in the eastern cordillera of colombia interpreted from fission track results and structural relationships: Implications for petroleum systems. *AAPG bulletin*, 94(10), 1543–1580.
- Mudd, S. M., Attal, M., Milodowski, D. T., Grieve, S. W., & Valters, D. A. (2014). A statistical framework to quantify spatial variation in channel gradients using the integral method of channel profile analysis. *Journal of Geophysical Research: Earth Surface*, 119(2), 138–152.
- Noriega-Londoño, S., Restrepo-Moreno, S. A., Vinasco, C., Bermúdez, M. A., & Min, K. (2020). Thermochronologic and geomorphometric constraints on the cenozoic landscape evolution of the northern andes: Northwest-central cordillera, colombia. *Geomorphology*, 351. doi: 10.1016/j.geomorph.2019.106890
- Ott, R. F., Pérez-Consegra, N., Scherler, D., Mora, A., Huppert, K. L., Braun, J., ... Ruiz, J. R. S. (2023). Erosion rate maps highlight spatio-temporal patterns of uplift and quantify sediment export of the northern andes. *Earth and Planetary Science Letters*, 621, 118354.
- Page, W. D. (1986). *Seismic geology and seismicity of northwestern colombia*. woodward-clyde consultants.

- Pedregosa, F., Varoquaux, G., Gramfort, A., Michel, V., Thirion, B., Grisel, O., ...
 626
 Duchesnay, E. (2011). Scikit-learn: Machine learning in Python. *Journal of*
 627 *Machine Learning Research*, 12, 2825–2830.
 628
- Pérez-Consuegra, N., Hoke, G., Fitzgerald, P., Mora, A., Sobel, E., & Glodny, J.
 629 (2022). Late miocene–pliocene onset of fluvial incision of the cauca river
 630 canyon in the northern andes. *Bulletin*, 134(9-10), 2453–2468.
 631
- Pérez-Consuegra, N., Ott, R. F., Hoke, G. D., Galve, J. P., Pérez-Peña, V., & Mora,
 632 A. (2021). Neogene variations in slab geometry drive topographic change
 633 and drainage reorganization in the northern andes of colombia. *Global and*
 634 *Planetary Change*, 206, 103641.
 635
- Pérez-Peña, J. V., Azañón, J. M., & Azor, A. (2009). CalHypso: An ArcGIS
 636 extension to calculate hypsometric curves and their statistical moments. Appli-
 637 cations to drainage basin analysis in SE Spain. *Computers and Geosciences*,
 638 35(6), 1214–1223. doi: 10.1016/j.cageo.2008.06.006
 639
- Perron, J. T., & Royden, L. (2013). An integral approach to bedrock river profile
 640 analysis. *Earth surface processes and landforms*, 38(6), 570–576.
 641
- Poveda, G., Alvarez, D. M., & Rueda, O. A. (2011). Hydro-climatic variability
 642 over the andes of colombia associated with enso: a review of climatic processes
 643 and their impact on one of the earth’s most important biodiversity hotspots.
 644 *Climate Dynamics*, 36, 2233–2249.
 645
- Poveda, G., & Mesa, O. J. (2000). On the existence of Iloró (the雨iest locality on
 646 earth): Enhanced ocean-land-atmosphere interaction by a low-level jet. *Geo-*
 647 *physical research letters*, 27(11), 1675–1678.
 648
- Reichenbach, P., Rossi, M., Malamud, B. D., Mihir, M., & Guzzetti, F. (2018). A
 649 review of statistically-based landslide susceptibility models. *Earth-science re-*
 650 *views*, 180, 60–91.
 651
- Restrepo-Moreno, S. A., Foster, D. A., Bernet, M., Min, K., & Noriega, S. (2019).
 652 Morphotectonic and orogenic development of the northern andes of colombia:
 653 A low-temperature thermochronology perspective. *Geology and Tectonics*
 654 *of Northwestern South America: The Pacific-Caribbean-Andean Junction*,
 655 749–832.
 656
- Roering, J. J., Mackey, B. H., Handwerger, A. L., Booth, A. M., Schmidt, D. A.,
 657 Bennett, G. L., & Cerovski-Darriaux, C. (2015). Beyond the angle of repose: A
 658 review and synthesis of landslide processes in response to rapid uplift, eel river,
 659 northern california. *Geomorphology*, 236, 109–131.
 660
- Rousseeuw, P. J. (1987). Silhouettes: a graphical aid to the interpretation and val-
 661 idation of cluster analysis. *Journal of computational and applied mathematics*,
 662 20, 53–65.
 663
- Schwanghart, W., & Scherler, D. (2014). TopoToolbox 2 – MATLAB-based software
 664 for topographic analysis and modeling in Earth surface sciences. *Earth Surface*
 665 *Dynamics*, 2, 1–7. doi: 10.5194/esurf-2-1-2014
 666
- Smith, R. B. (2006). Progress on the theory of orographic precipitation.
 667 Soeters, R., & Van Westen, C. (1996). Slope instability recognition, analysis and
 668 zonation. *Landslides: investigation and mitigation*, 247, 129–177.
 669
- Stock, J. D., & Montgomery, D. R. (1999). Geologic constraints on bedrock river
 670 incision using the stream power law. *Journal of Geophysical Research: Solid*
 671 *Earth*, 104(B3), 4983–4993.
 672
- Strahler, A. N. (1952). Hypsometric (area-altitude) analysis of erosional topography.
 673 *Bulletin of the Geological Society of America*, 63(11), 1117–1142. doi: 10.1130/
 674 0016-7606(1952)63[1117:HAAOET]2.0.CO;2
 675
- Taboada, A., Rivera, L. A., Fuenzalida, A., Cisternas, A., Philip, H., Bijwaard, H.,
 676 ... Rivera, C. (2000). Geodynamics of the northern andes: Subductions and
 677 intracontinental deformation (colombia). *Tectonics*, 19(5), 787–813.
 678
- Thorndike, R. L. (1953). Who belongs in the family? *Psychometrika*, 18(4), 267–
 679 276.
 680

- 681 Trenkamp, R., Kellogg, J. N., Freymueller, J. T., & Mora, H. P. (2002). Wide plate
682 margin deformation, southern Central America and northwestern South Amer-
683 ica, CASA GPS observations. *Journal of South American Earth Sciences*,
684 15(2), 157–171. doi: 10.1016/S0895-9811(02)00018-4
- 685 Tsou, C. Y., Chigira, M., Matsushi, Y., Hiraishi, N., & Arai, N. (2017, 12). Cou-
686 pling fluvial processes and landslide distribution toward geomorphological
687 hazard assessment: a case study in a transient landscape in japan. *Landslides*,
688 14, 1901-1914. doi: 10.1007/s10346-017-0838-3
- 689 Whipple, K. X. (2002). Implications of sediment-flux-dependent river incision mod-
690 els for landscape evolution. *Journal of Geophysical Research*, 107. doi: 10
691 .1029/2000jb000044
- 692 Whipple, K. X. (2004). Bedrock rivers and the geomorphology of active orogens.
693 *Annu. Rev. Earth Planet. Sci.*, 32, 151–185.
- 694 Whipple, K. X., Forte, A., DiBiase, R., Gasparini, N., & Ouimet, W. (2017).
695 Timescales of landscape response to divide migration and drainage capture:
696 Implications for the role of divide mobility in landscape evolution. *Journal of*
697 *Geophysical Research: Earth Surface*, 122(1), 248–273.
- 698 Whittaker, A. C. (2012, 04). How do landscapes record tectonics and climate?
699 *Lithosphere*, 4(2), 160-164. Retrieved from <https://doi.org/10.1130/RF.L003.1>
700 doi: 10.1130/RF.L003.1
- 701 Willett, S. D., McCoy, S. W., Perron, J. T., Goren, L., & Chen, C.-Y. (2014). Dy-
702 namic reorganization of river basins. *Science*, 343(6175), 1248765.
- 703 Wobus, C. W., Whipple, K. X., Kirby, E., Snyder, N. P., Johnson, J. P. L., Spy-
704 ropolou, K., ... Sheehan, D. D. (2006). Tectonics from topography:
705 Procedures, promise, and pitfalls. *Special Paper of the Geological Soci-
706 ety of America* 398, *Tectonics, Climate, and Landscape Evolution, Sean*
707 *D. Willett, Niels Hovius, Mark T. Brandon, Donald M. Fisher.* doi:
708 [https://doi.org/10.1130/2006.2398\(04\)](https://doi.org/10.1130/2006.2398(04))
- 709 Yanites, B. J., Mitchell, N. A., Bregy, J. C., Carlson, G. A., Cataldo, K., Holahan,
710 M., ... Wanket, M. (2018). Landslides control the spatial and temporal varia-
711 tion of channel width in southern taiwan: Implications for landscape evolution
712 and cascading hazards in steep, tectonically active landscapes. *Earth Surface*
713 *Processes and Landforms*, 43(9), 1782–1797.

Figure 1. Tectonic setting of the Colombian Andes. Cauca-Romeral Fault System (CRFS), Itsmina Deformation Zone (IDZ), Espíritu Santo Fault (ESF), Palestina Fault System (PFS), Uramita Fault system (UFS), Arma Fault (AF), Santa Marta-Bucaramanga Fault (SMBF), Algeciras Fault (AF). Arrows indicate contemporary plate vectors.

Figure 2. (A) Simplified geological map of the study area, modified from J. Gómez et al. (2015). (B) Normalized density of geological lineaments >1 km, estimated from eight hillshade directions with 45° -bins of azimuth at a sun elevation of 45° . Black lines are major active faults: Uramita Fault System (UFS), Espíritu Santo Fault (ESF), Arma Fault (AF), Cauca-Romeral Fault System (CRFS), Palestina Fault System (PFS), and Itsmina Deformation Zone (IDZ).

Figure 3. Mean annual rainfall (1981-2023) from CHIRPS data (Funk et al., 2015) in the study area. A, B and C are 10-km swath profiles, where black lines are mean elevation and red shades show 1-km local relief; blue bars are mean annual rainfall. The study area covers parts of the Central and Western Cordillera, separated by the Cauca canyon, and bounded by the Atrató and Magdalena rivers in the west and east, respectively.

Figure 4. Distribution of 222 prehistoric (of unknown dates) landslides and 13,777 recent landslides (known to have occurred between 1970 and 2023) in the study area; points mark the centroids of landslide scarps.

Figure 5. Distribution of recent (1970 to 2023) landslides (red crosses) and major knickpoints >100 m (bubbles) in the study area, and the Atrató, Cauca, and Magdalena basins (insets); bubble size scaled to vertical knickpoint height. Histograms show distributions of recent landslides and knickpoints in terms of elevation and distance from basin outlets; elevation refers to the center of the landslide scarp, while the distance to outlet corresponds to the nearest drainage that we projected this scarp point onto. Note how landslides can variably abound in areas without major knickpoints (entire study area); mainly above knickpoints (Atrató); or mainly below knickpoints (Cauca).

Figure 6. (A) Scatter plot of mean annual rainfall versus HI averaged for each of 650 catchments with corresponding box-and-whiskers for the study area (white); catchments with landslides (gray): catchments without landslides (green); with recent landslides (red); and with prehistoric landslides (black); symbol size scaled to the number of landslides in each catchment. Box-and-whisker plots show distributions of HI . Blue lines (and shades) are regression curves (and 95% confidence intervals) for Atrató and Magdalena basins. (B) Catchment-wide distribution of HI with superimposed landslide pattern.

Figure 7. Cluster analysis of catchment hypsometry reveals four distinct groups (A-D) shown here in map view (left) and as distributions of normalized elevation (color-coded lines, right; grey lines are raw data for each catchment). Clusters A to D identify groups of catchments with shifting dominance from lower to higher relative elevations.

Figure 8. Distributions of catchment-averaged topographic metrics, i.e. hypsometric integral HI , relief, slope, landslide density (Lands.), and mean annual rainfall P for each hypsometric cluster (Fig. 7). Box-and-whisker plots show medians with notches (95% confidence Interval); whiskers span 1.5 times the interquartile range; bubbles are outside this range. Note how the distributions of these metrics differ between clusters without having been part of the original cluster derivation.

Figure 9. River longitudinal profiles (blue), hypsometry (marginal histograms), and landslide distributions in sample catchments from clusters A, B, C and D each. Note the spatial proximity of the four catchments. Landslide outlet distance are projected to the closest drainage channel.

Figure 10. Distribution of χ along the drainage network of the northern Colombian Andes with prehistoric and recent landslides. Red lines are inferred actively migrating drainage divides between main catchments; red arrows indicate expected direction of catchment capture; T1 to T4 mark dominant divide migrating trends. Histograms show the distance of landslides from the nearest actively migrating drainage divide in 5-km bins, normalized by the fraction of study area at this distance; a relative frequency of 1 marks the expected value for a random distribution.

Figure1.

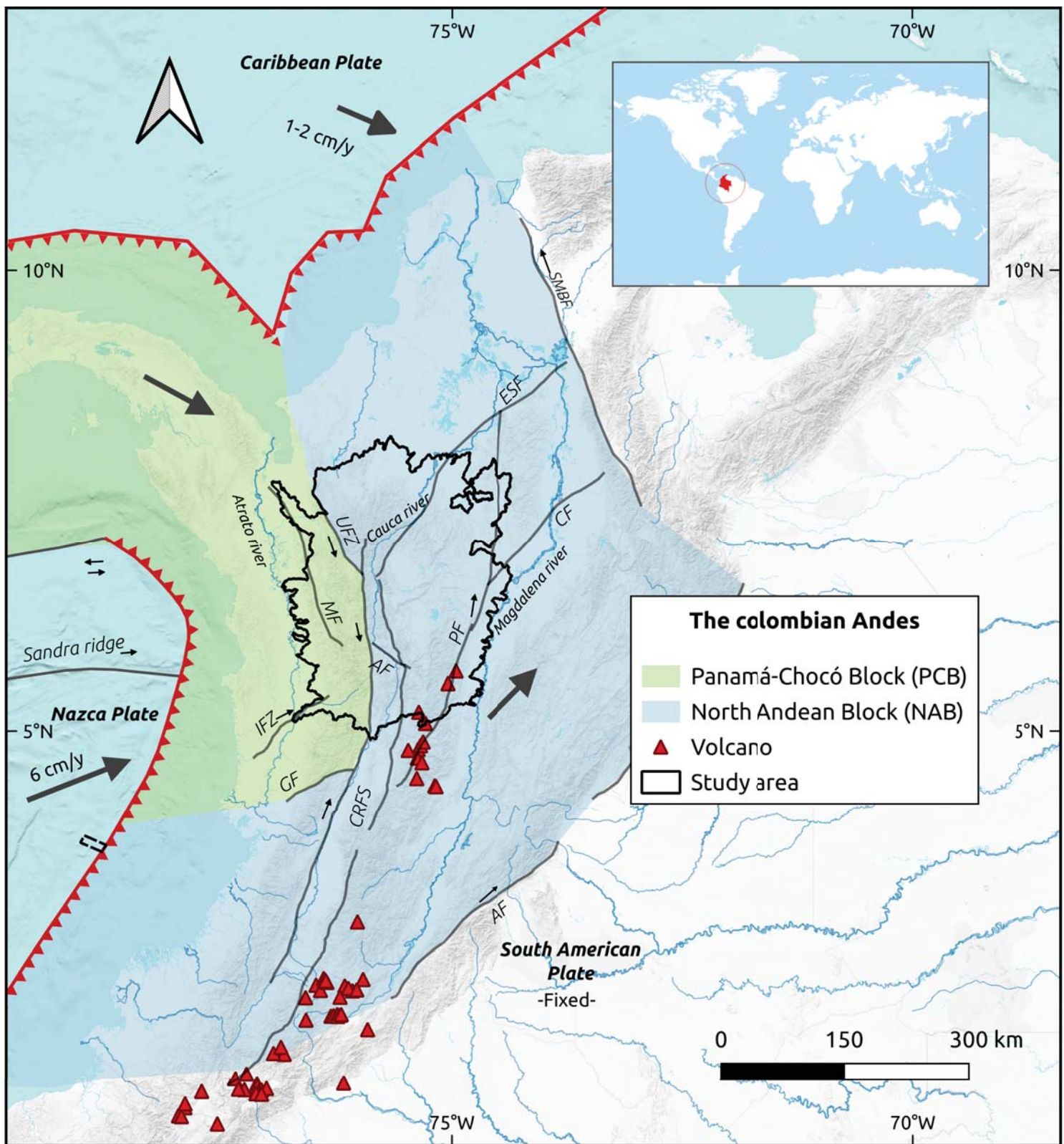


Figure2A.

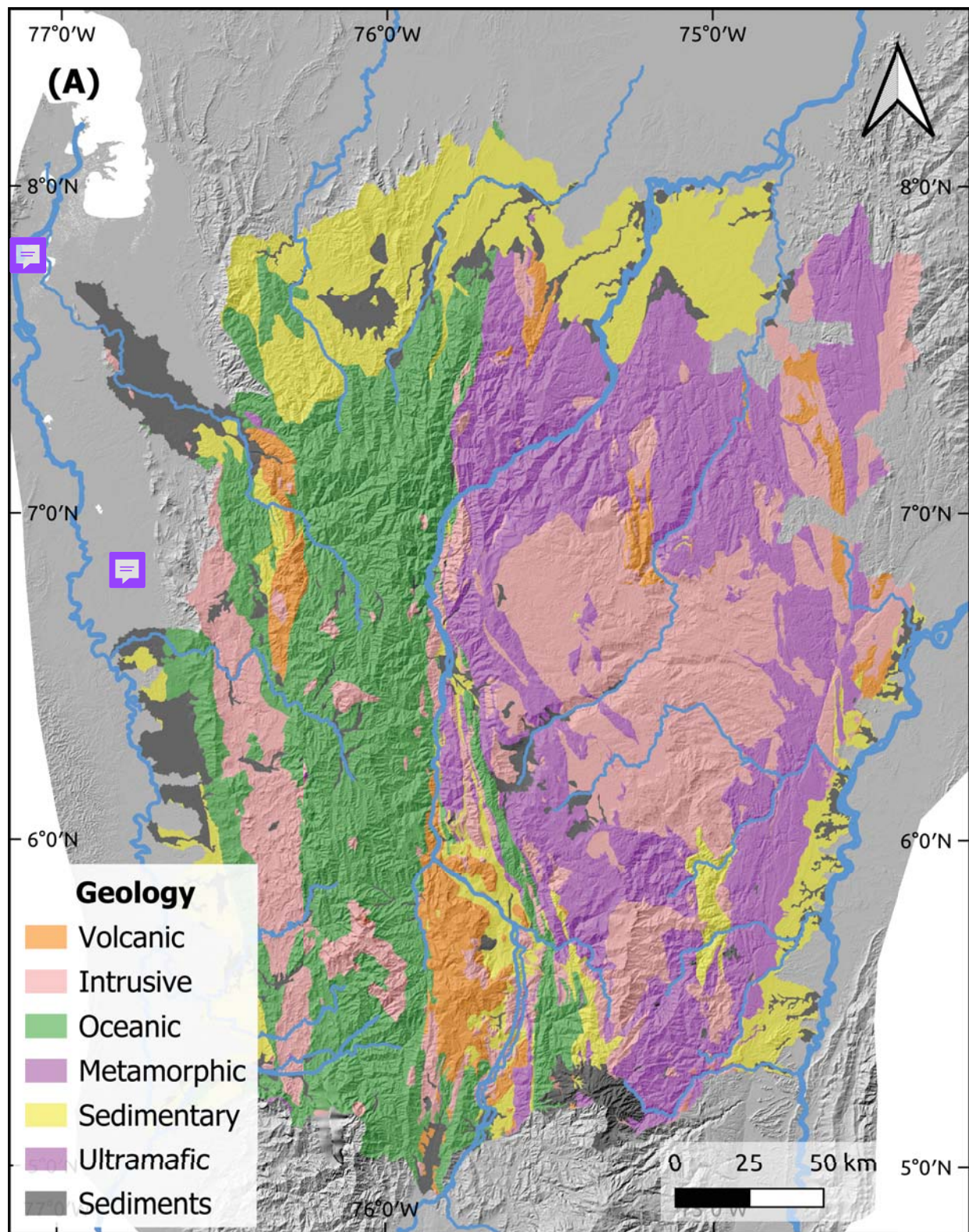


Figure2B.

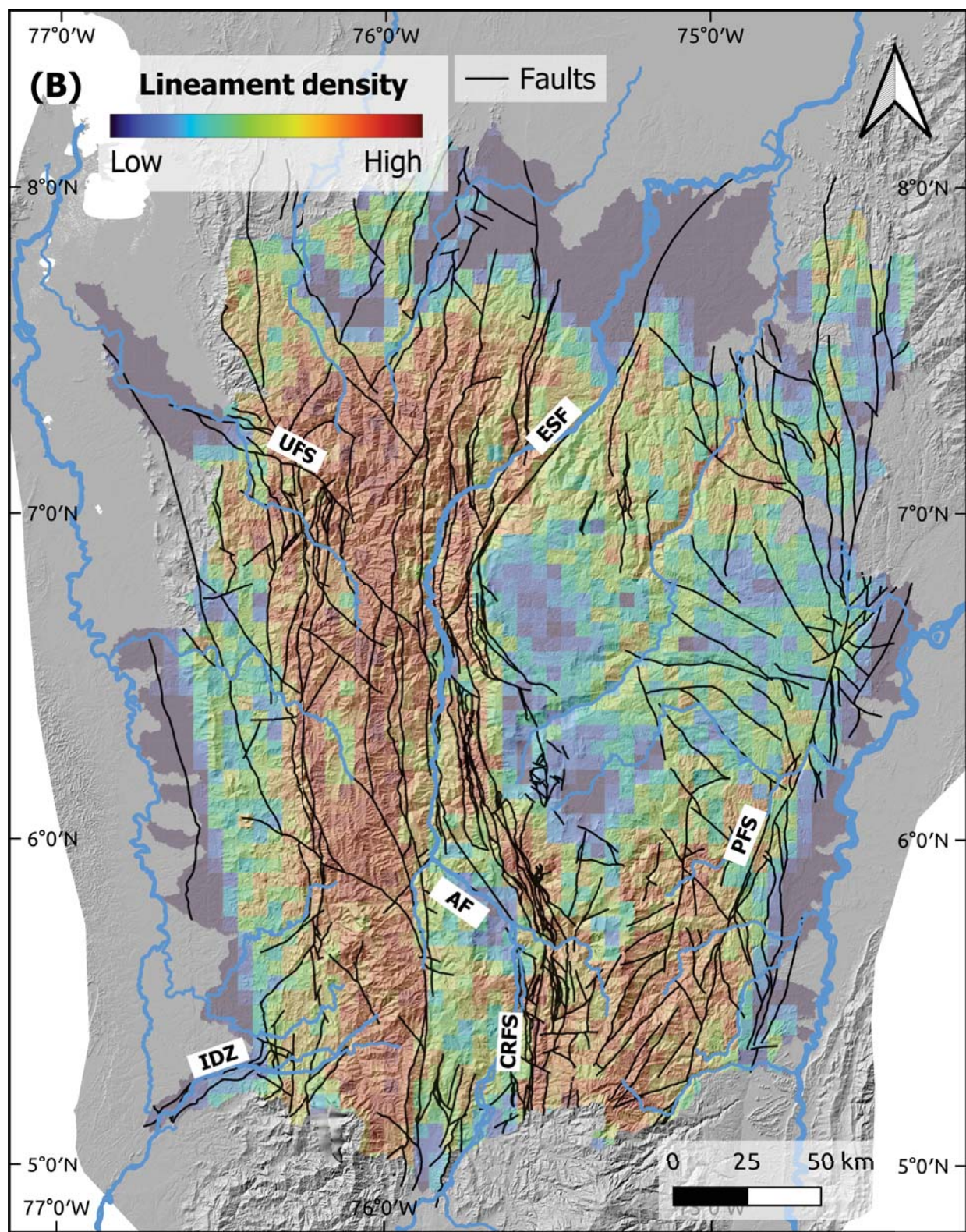


Figure3.

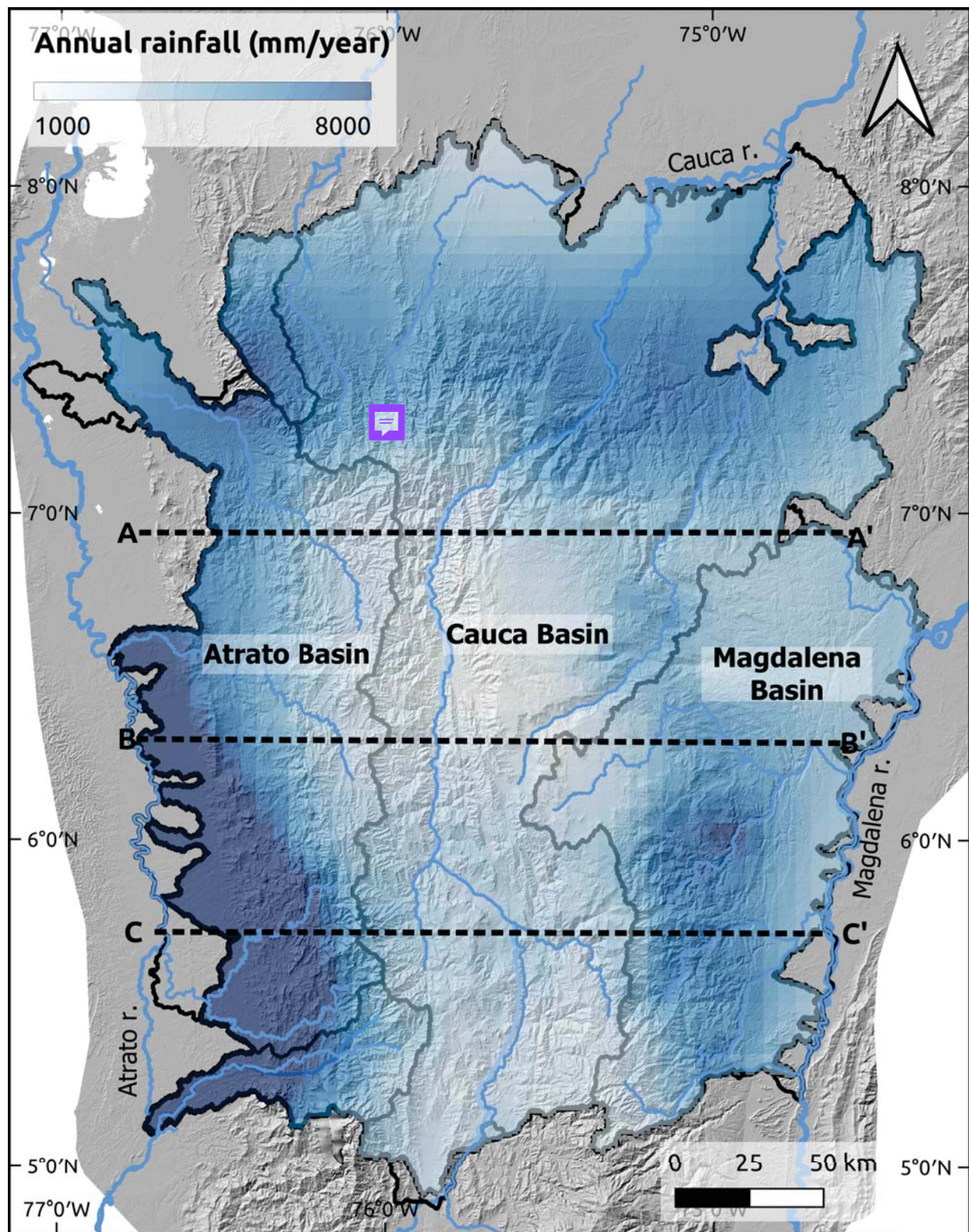


Figure3A.

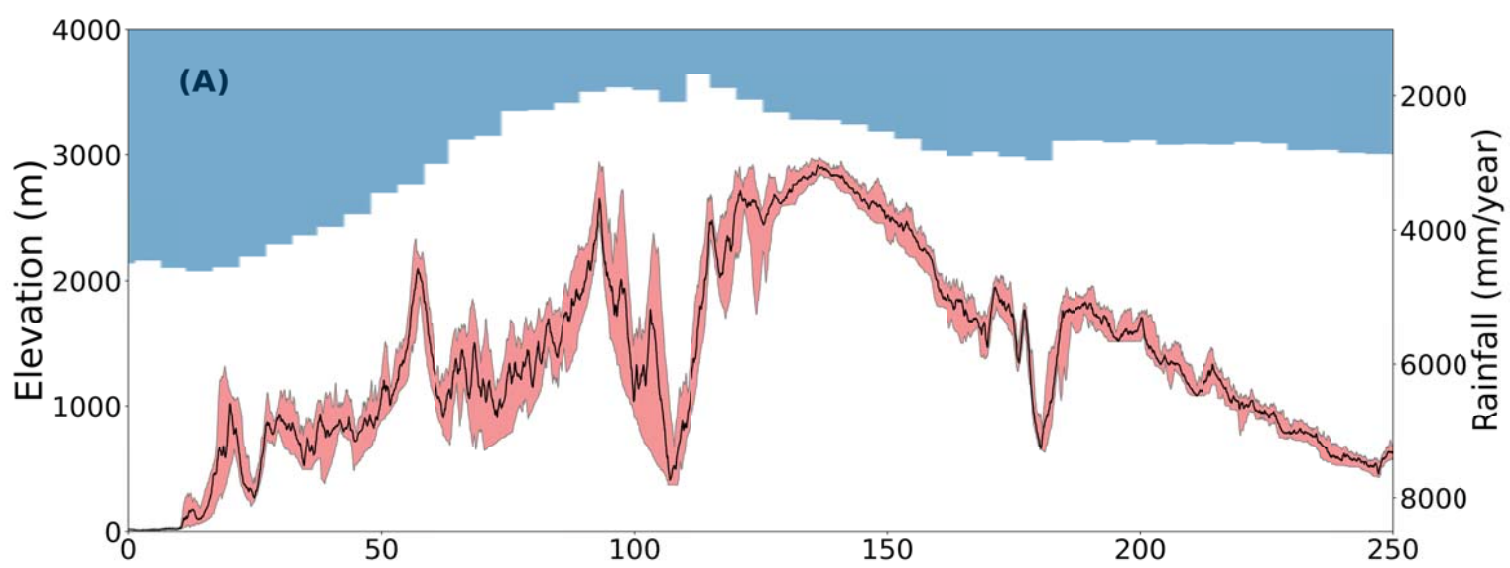


Figure3B.

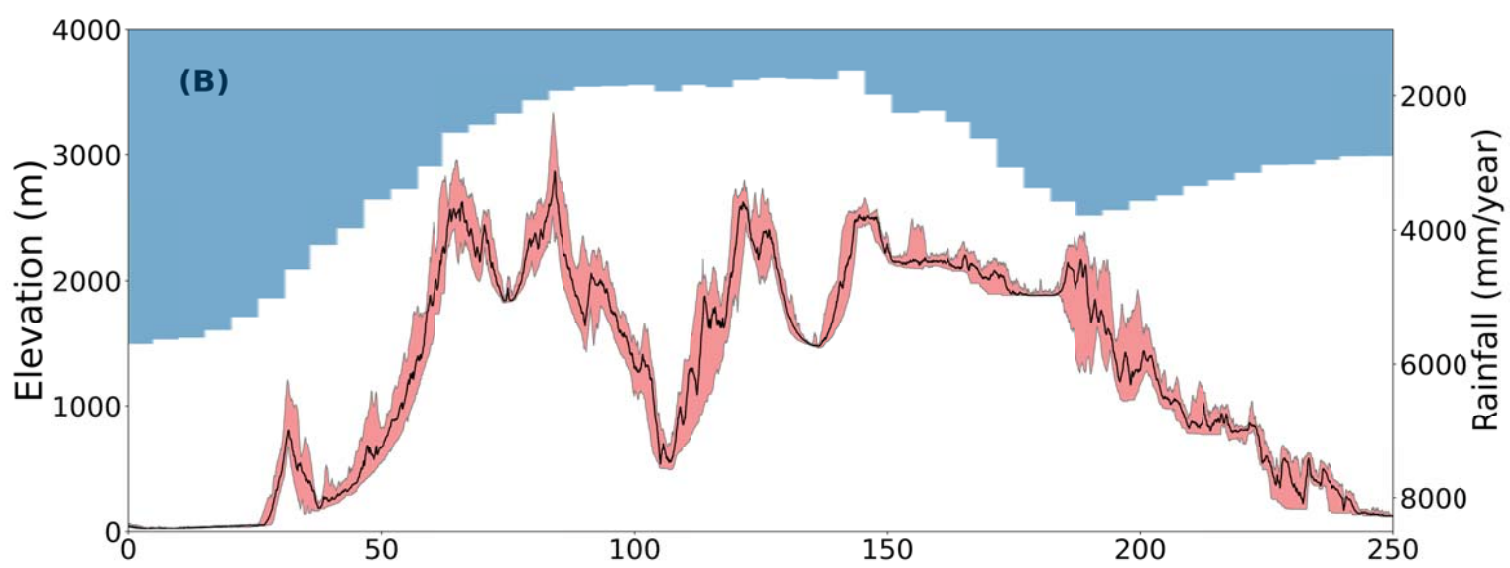


Figure3C.

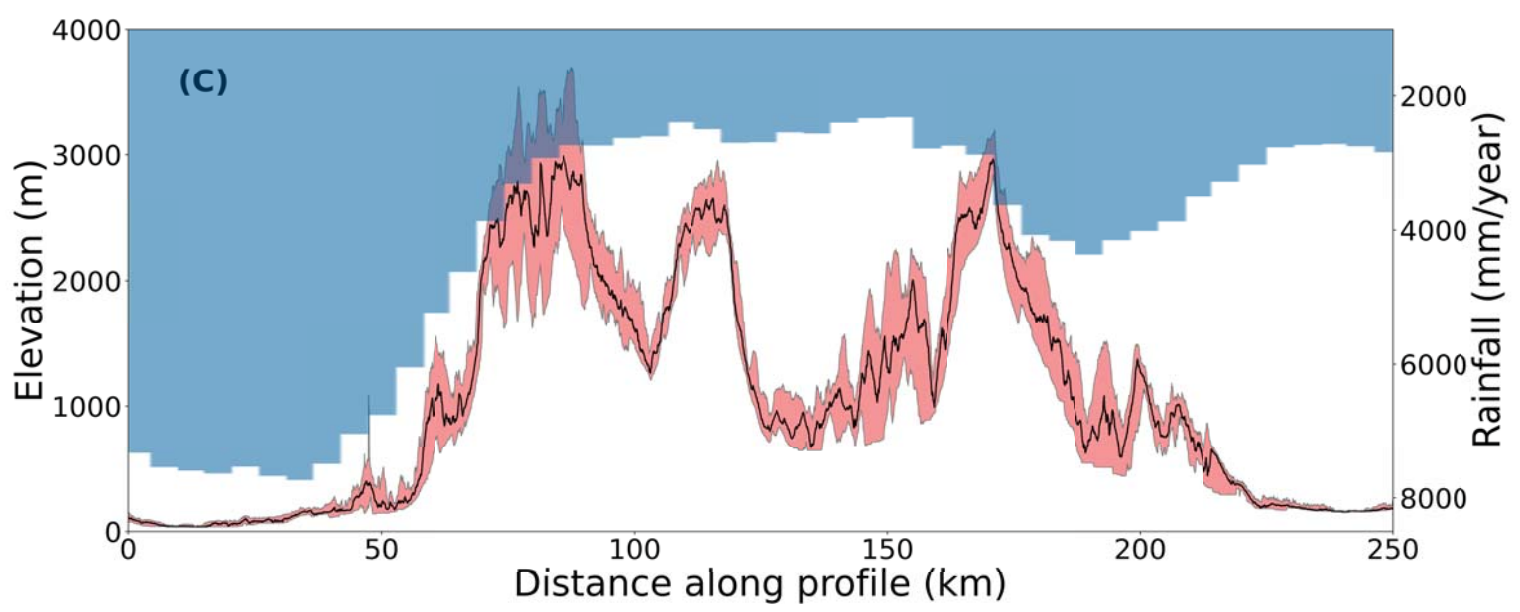


Figure4A.

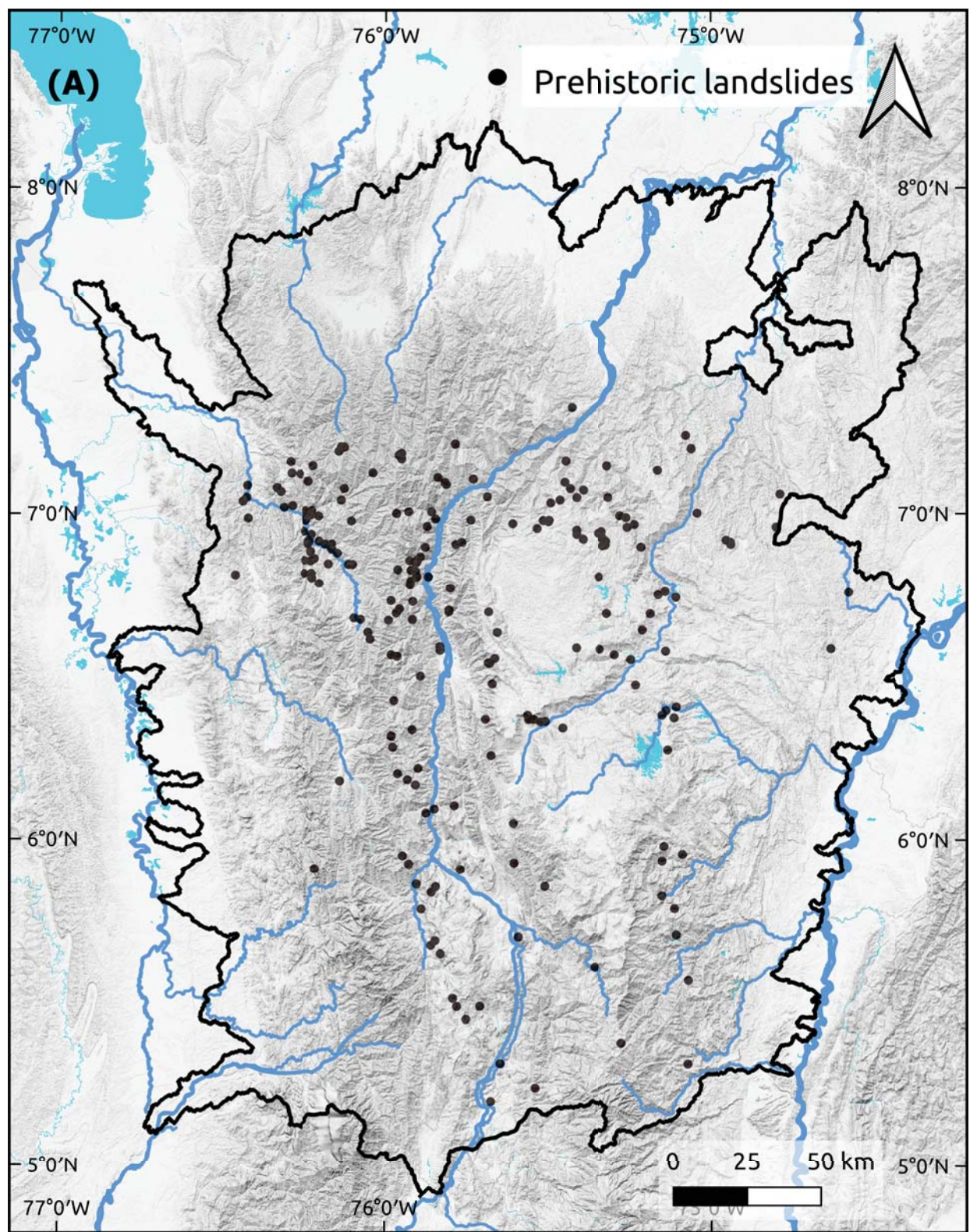


Figure4B.

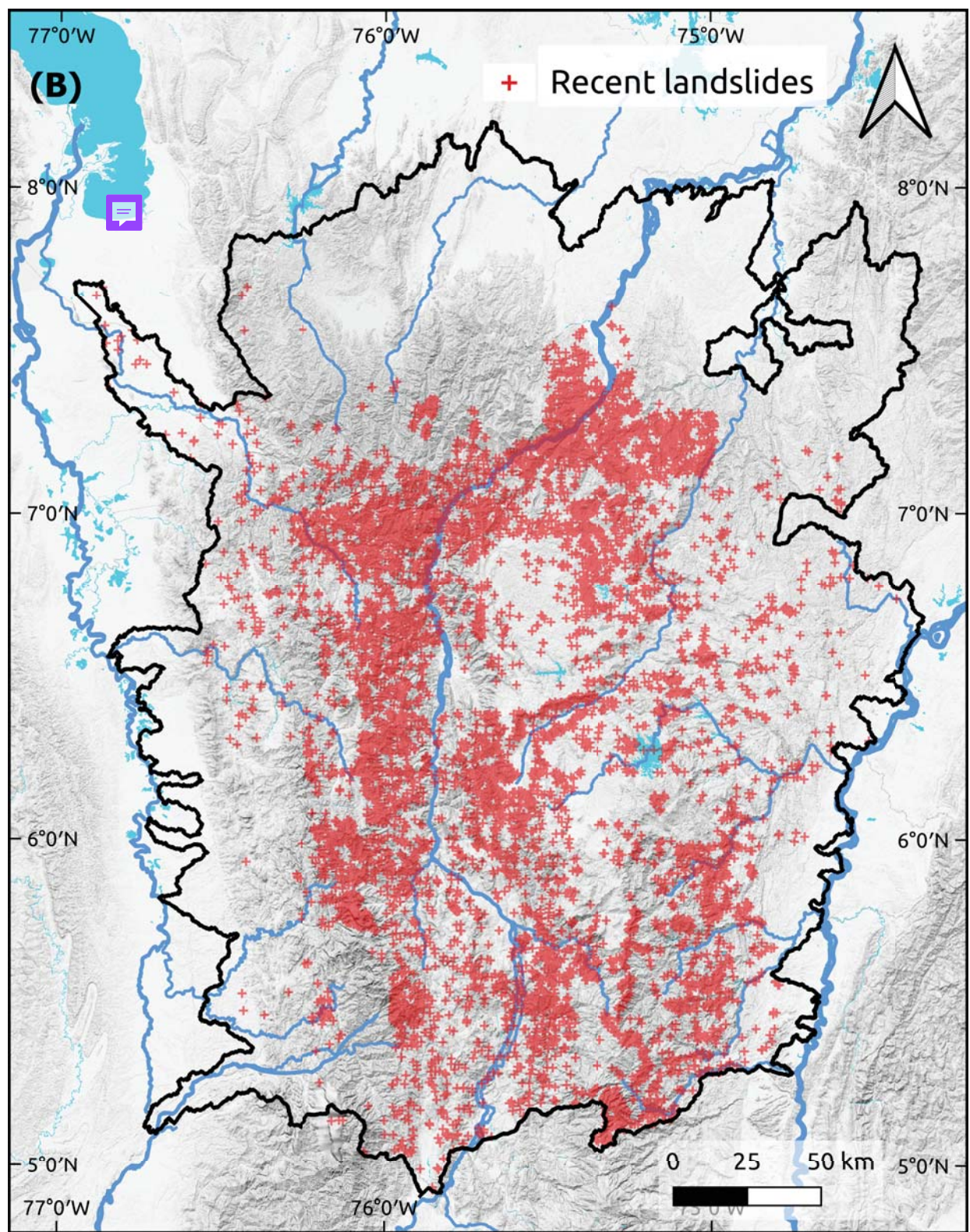


Figure5.

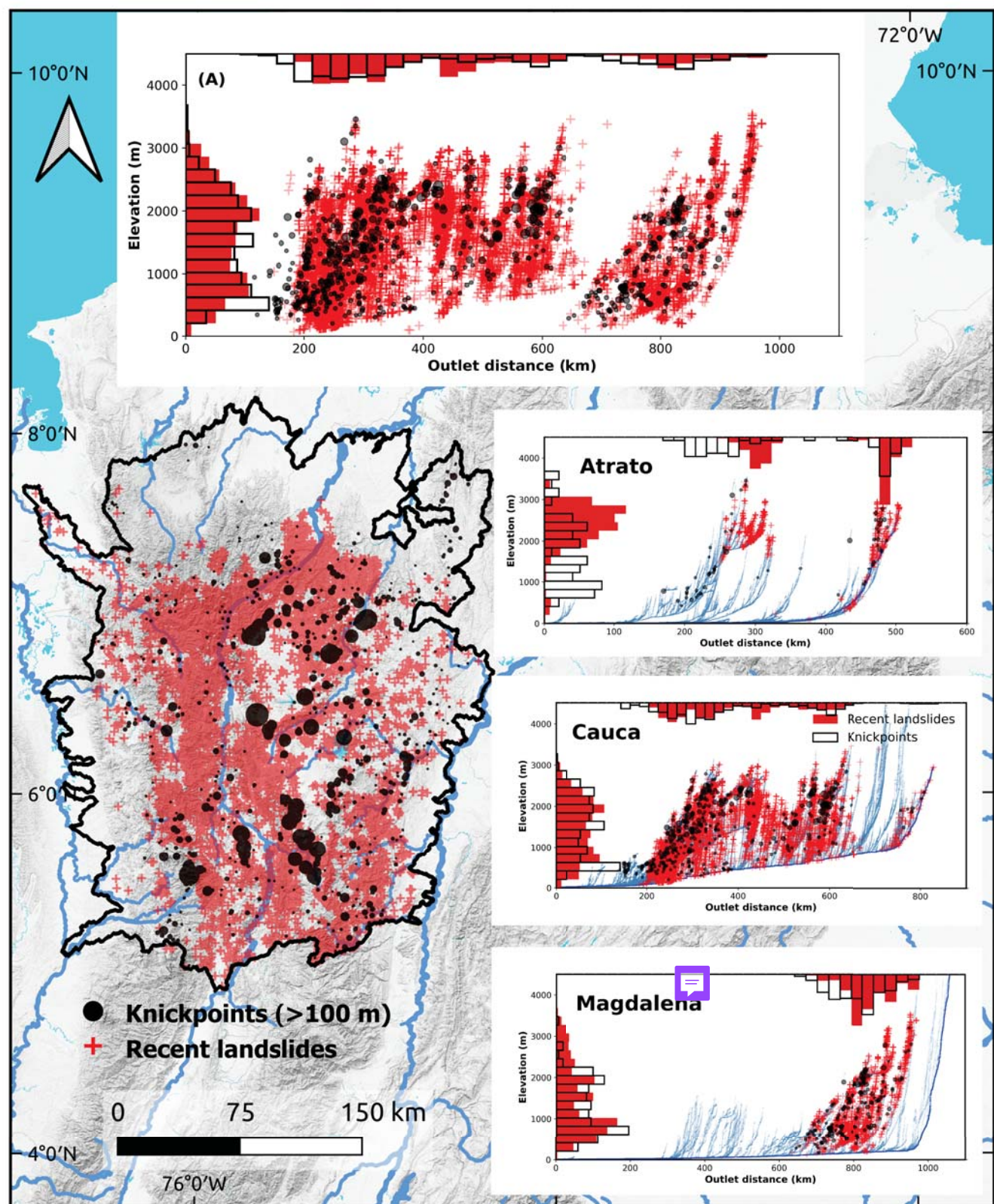


Figure6A.

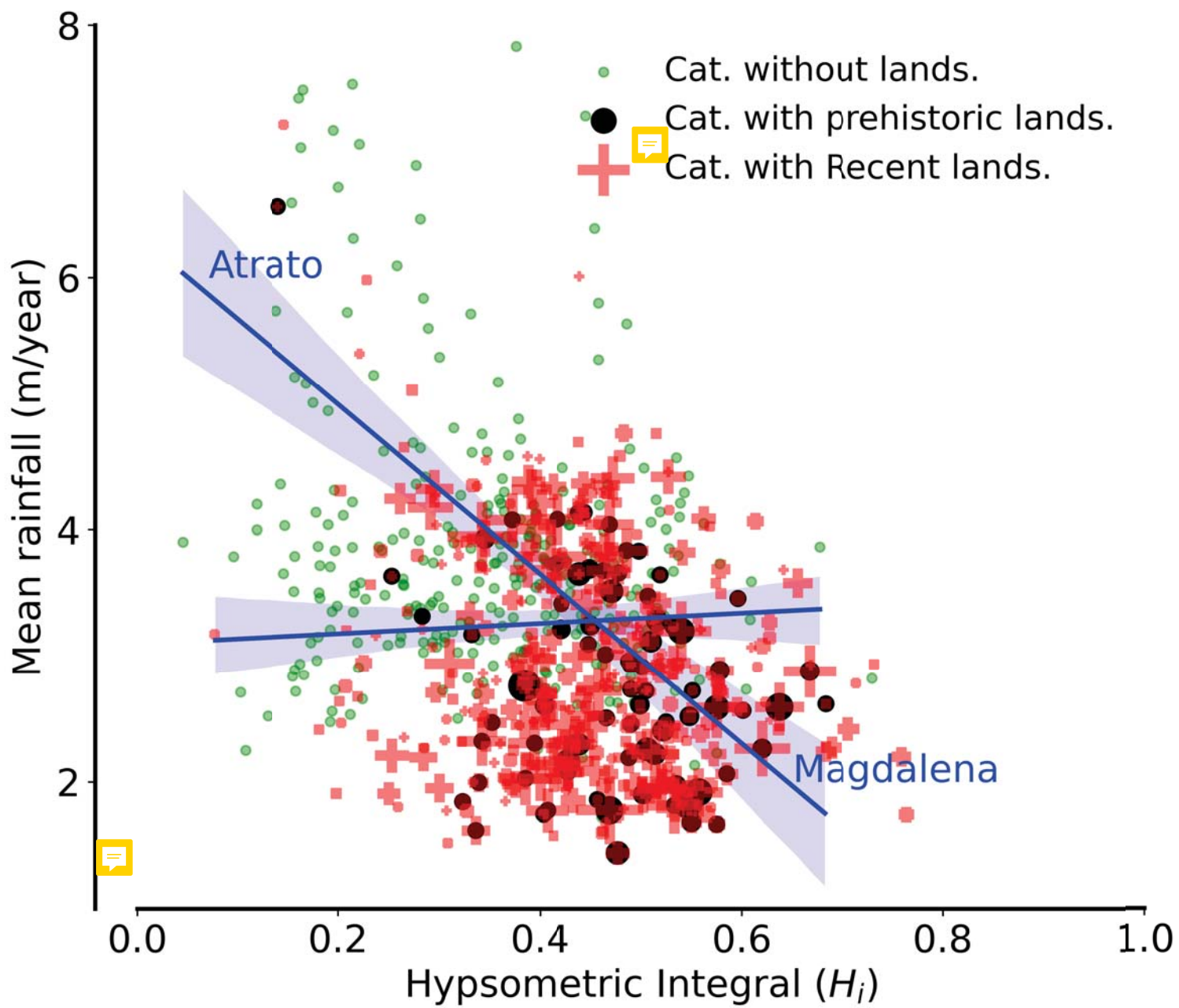
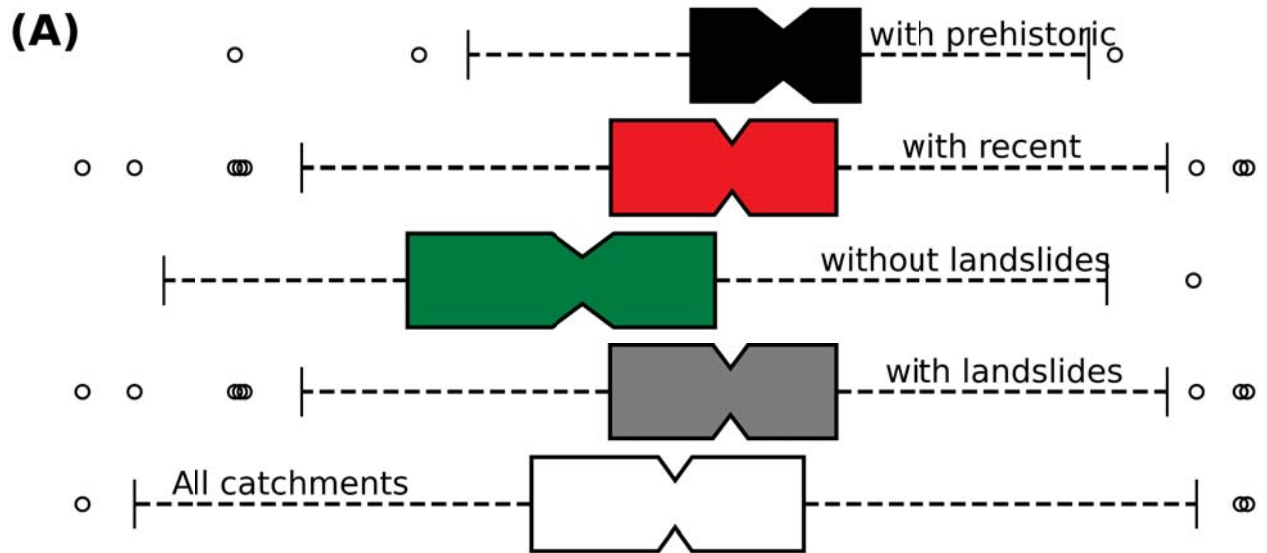


Figure6B.

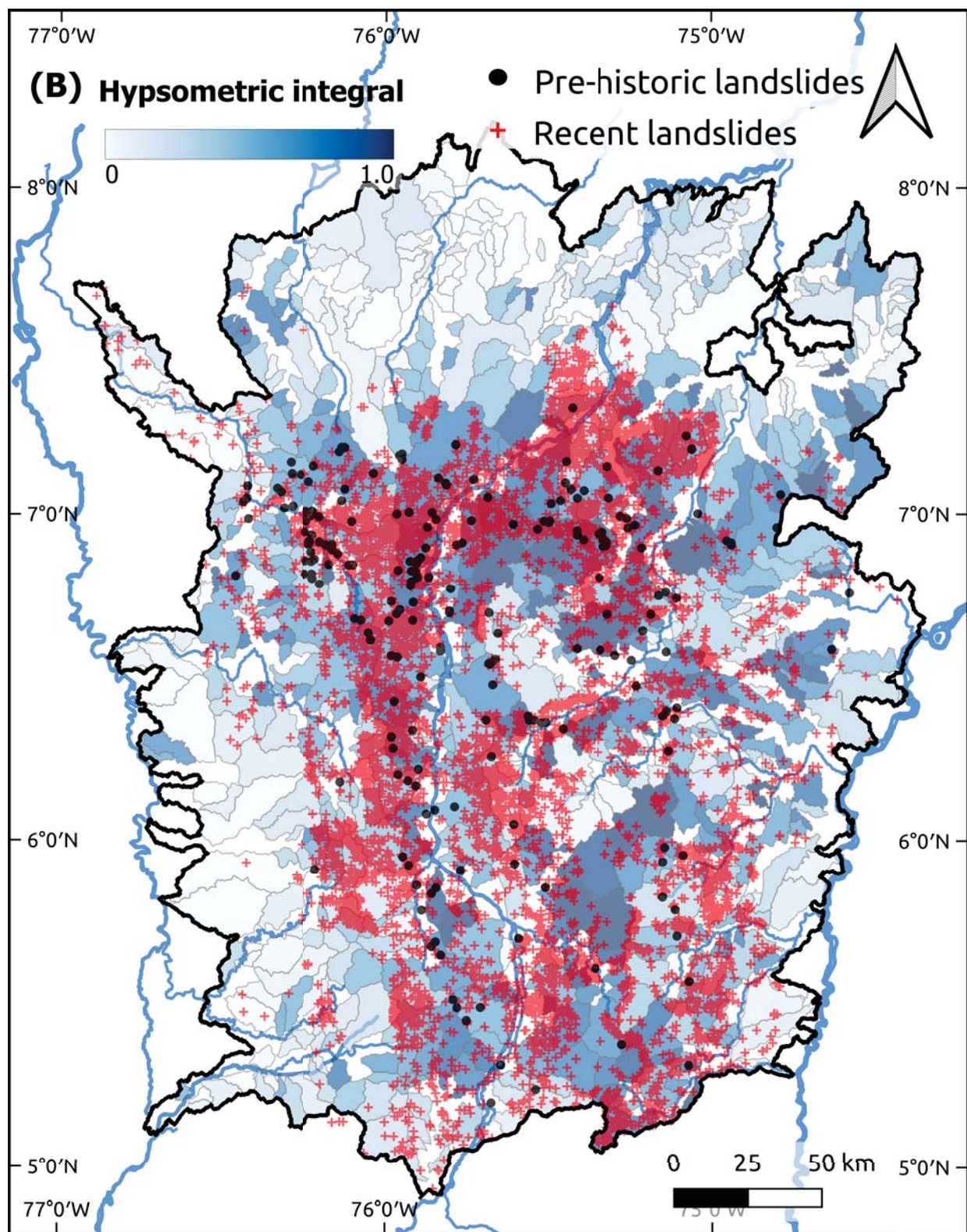


Figure7A.

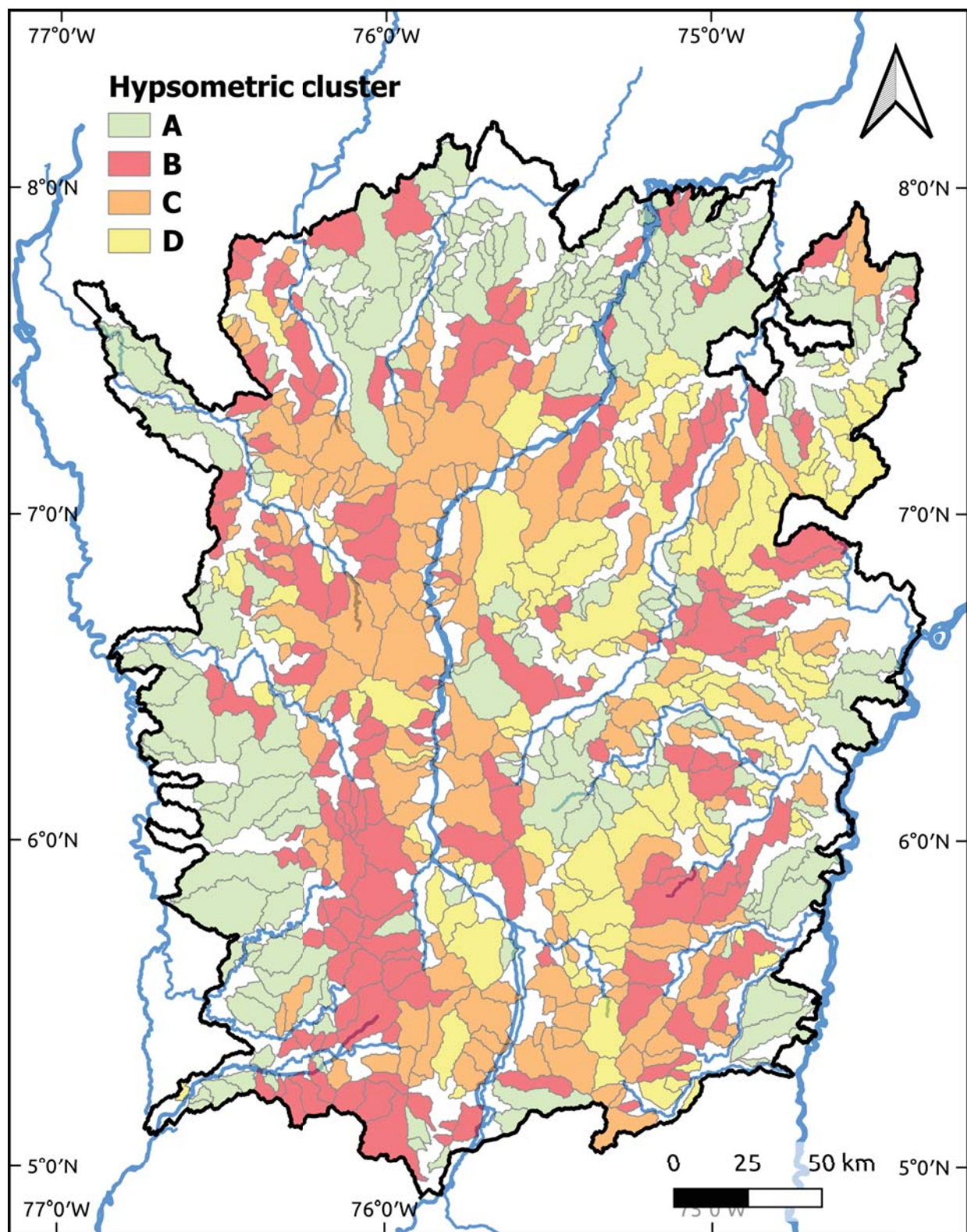


Figure7B.

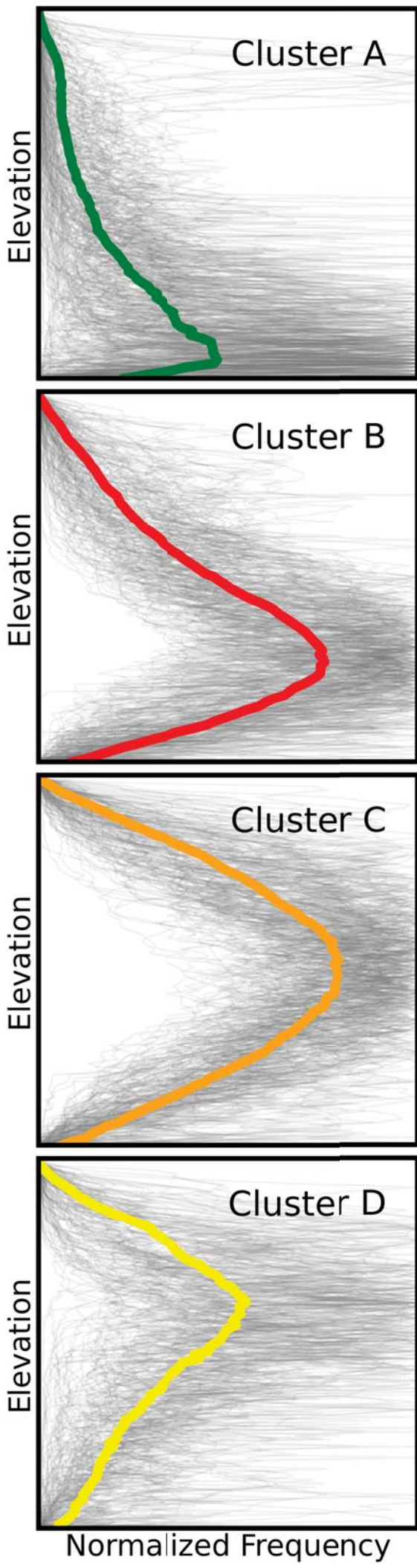


Figure8.

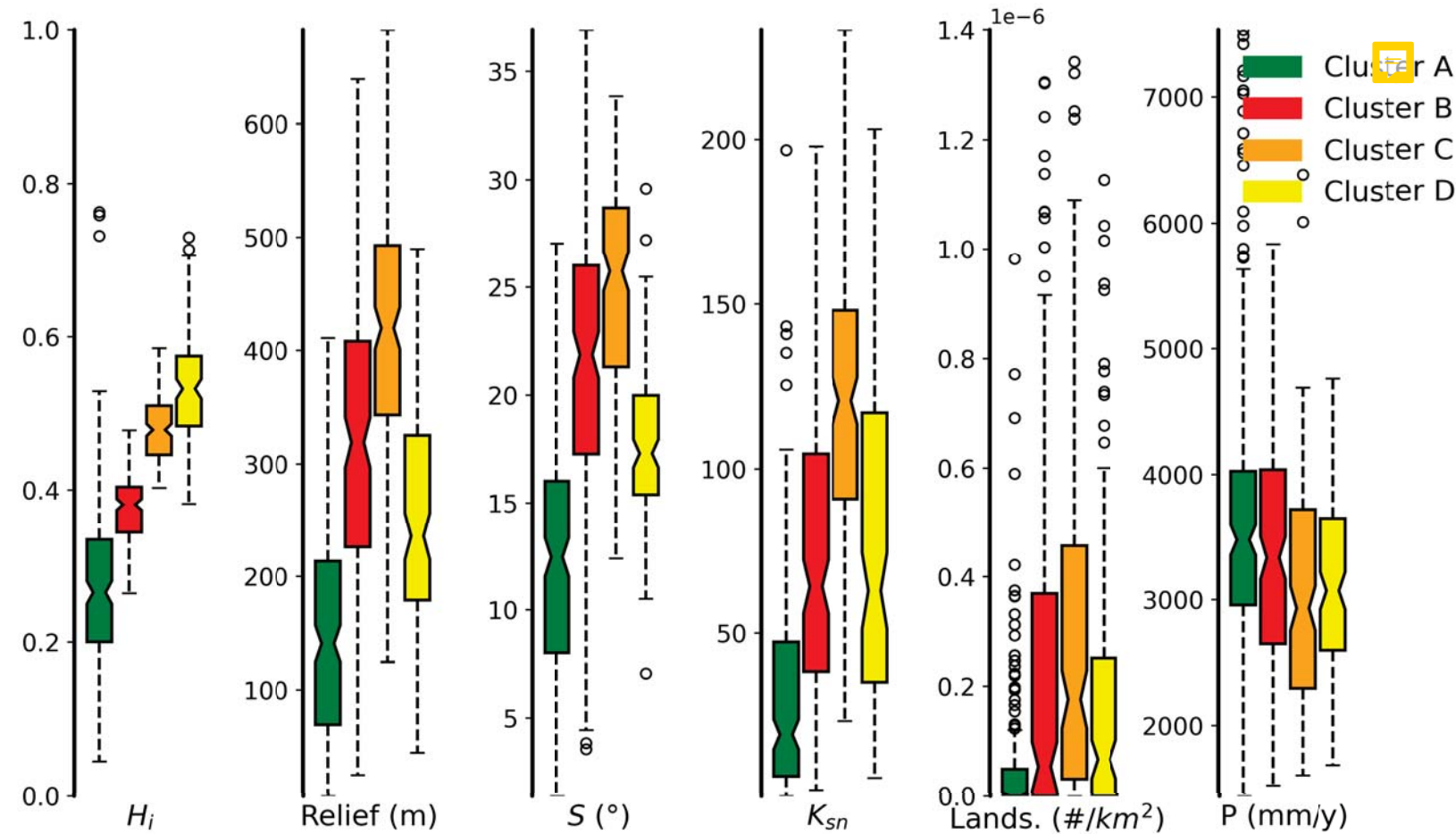


Figure9A.

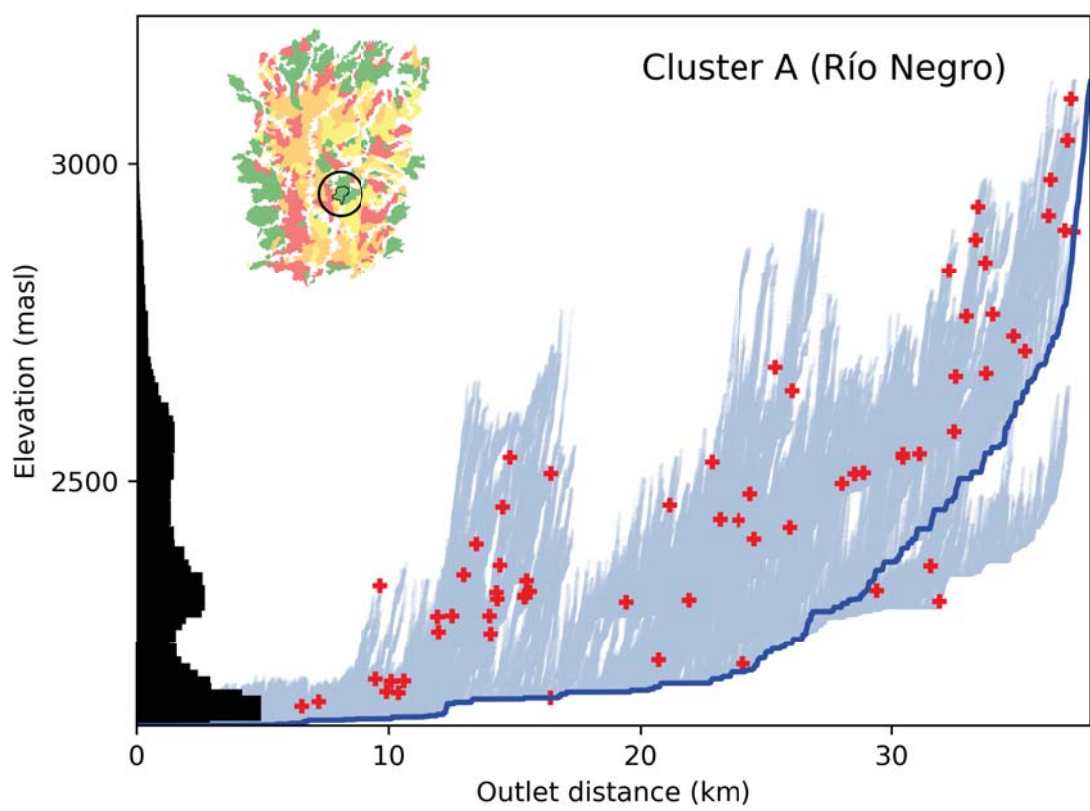


Figure9B.

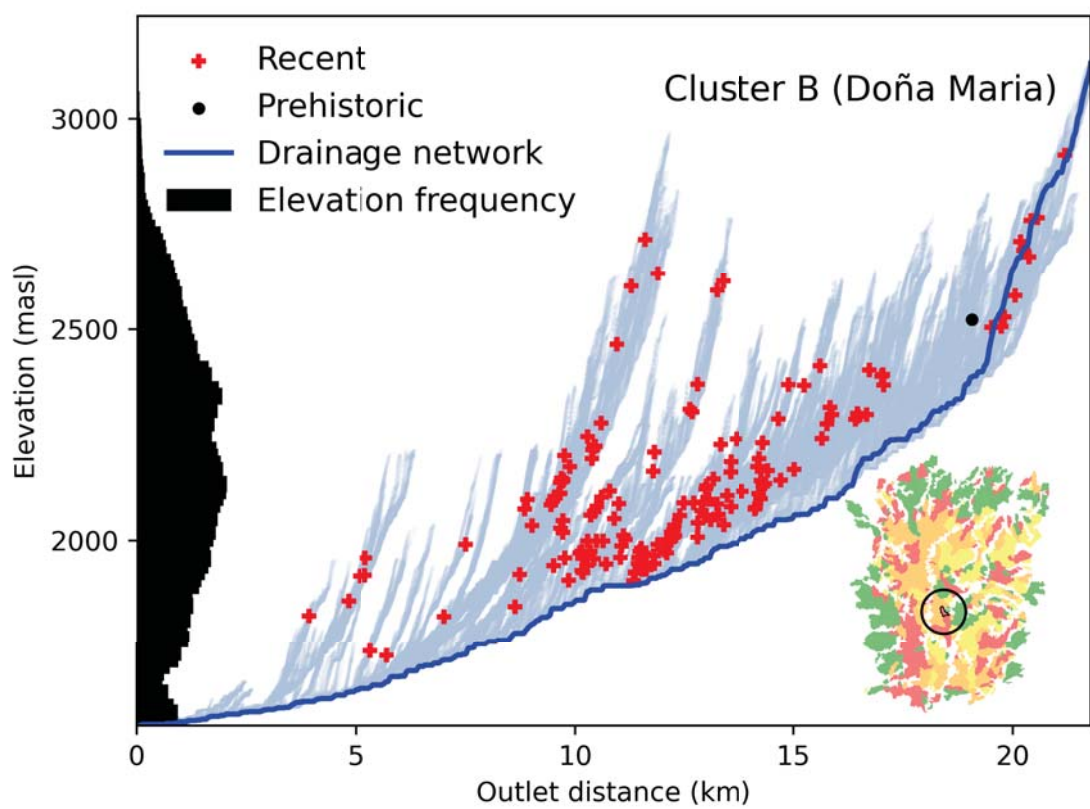


Figure9C.

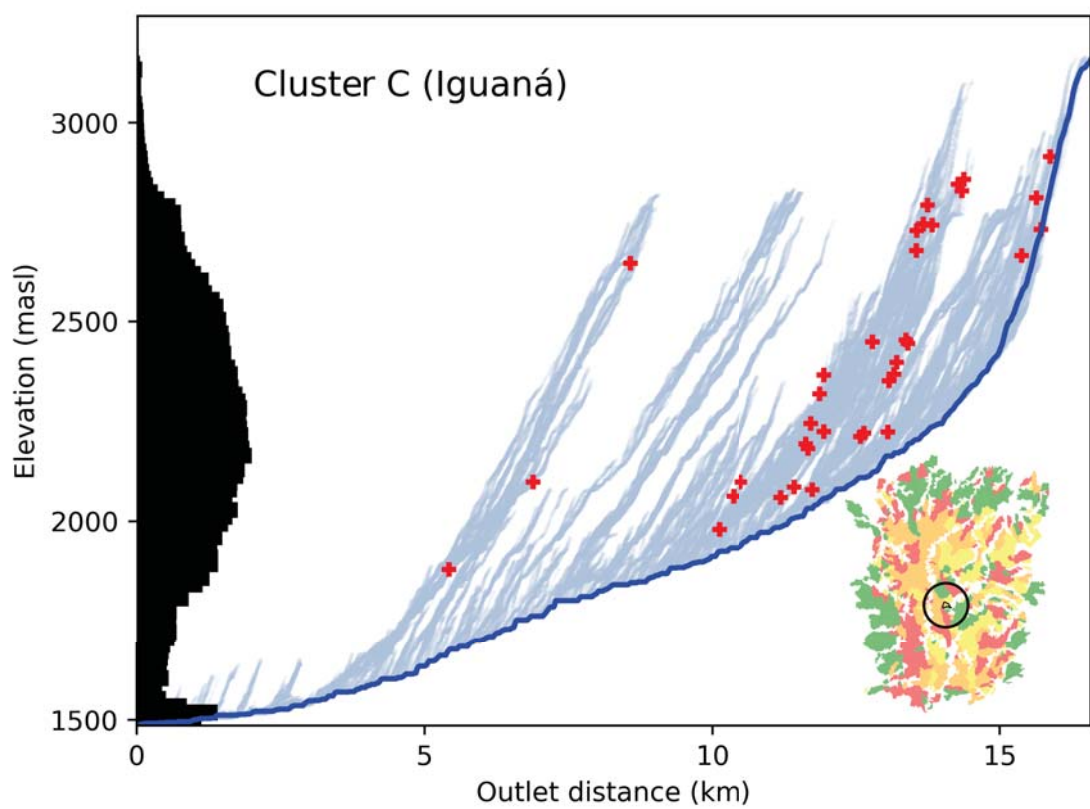


Figure9D.

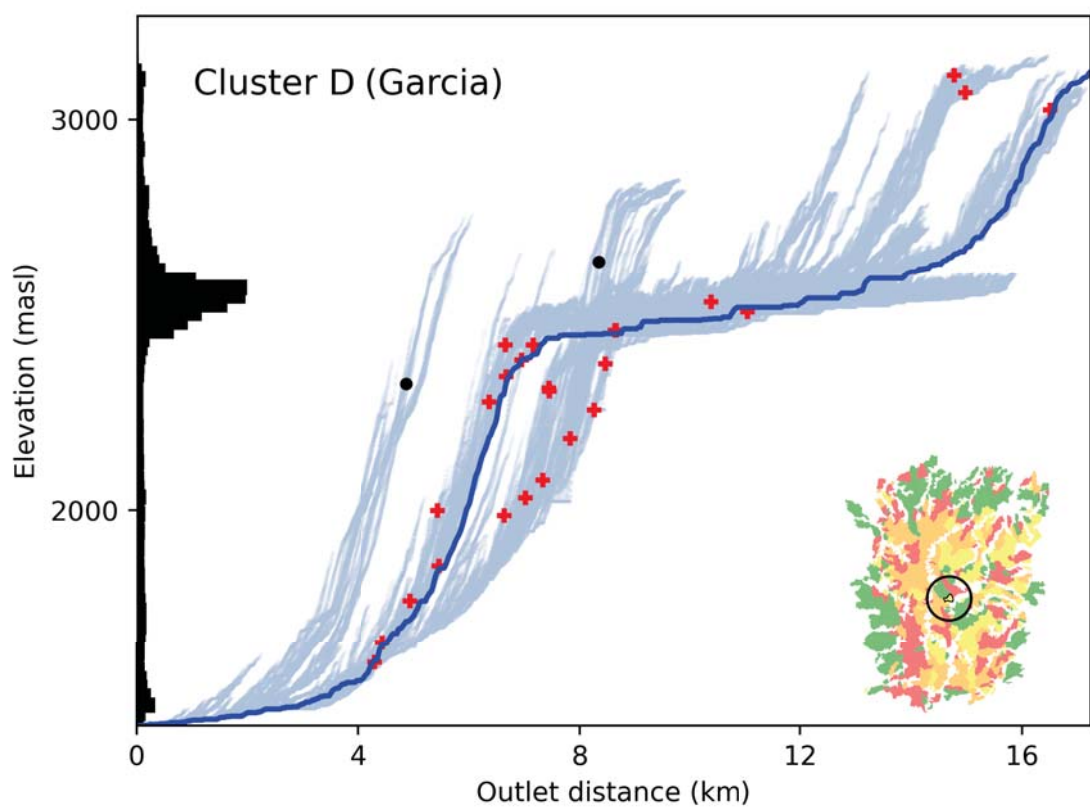


Figure10A.

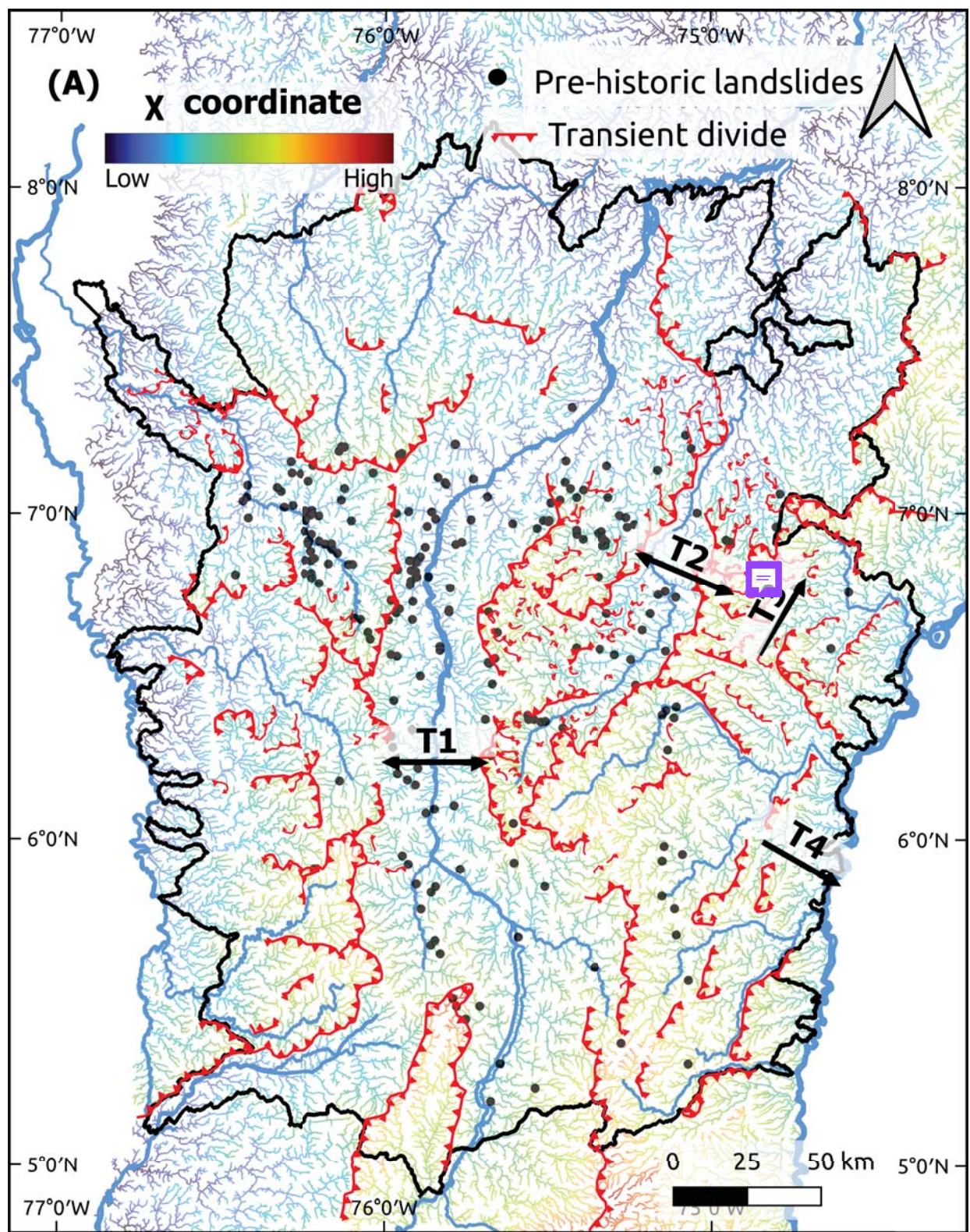


Figure10B.

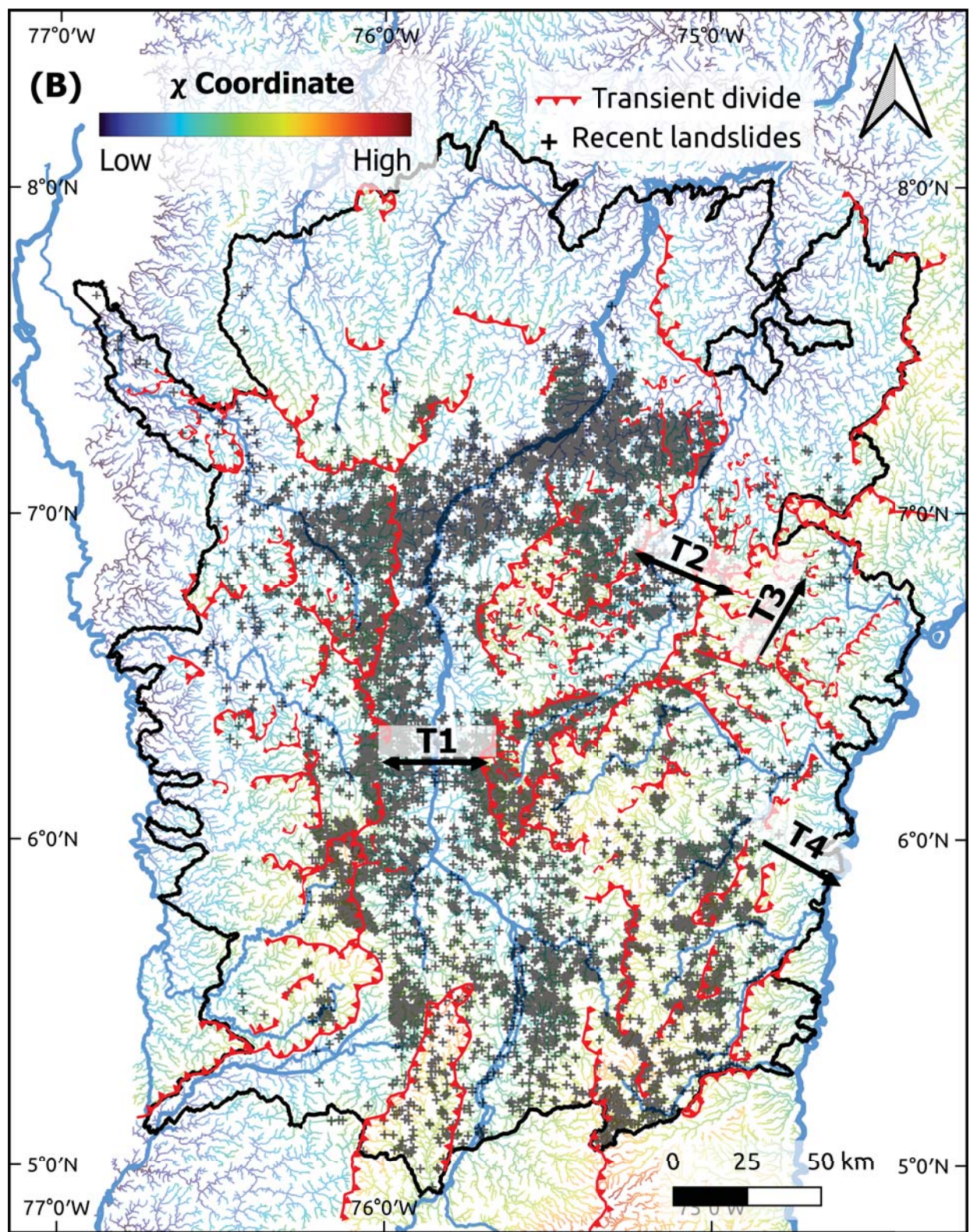


Figure10C.

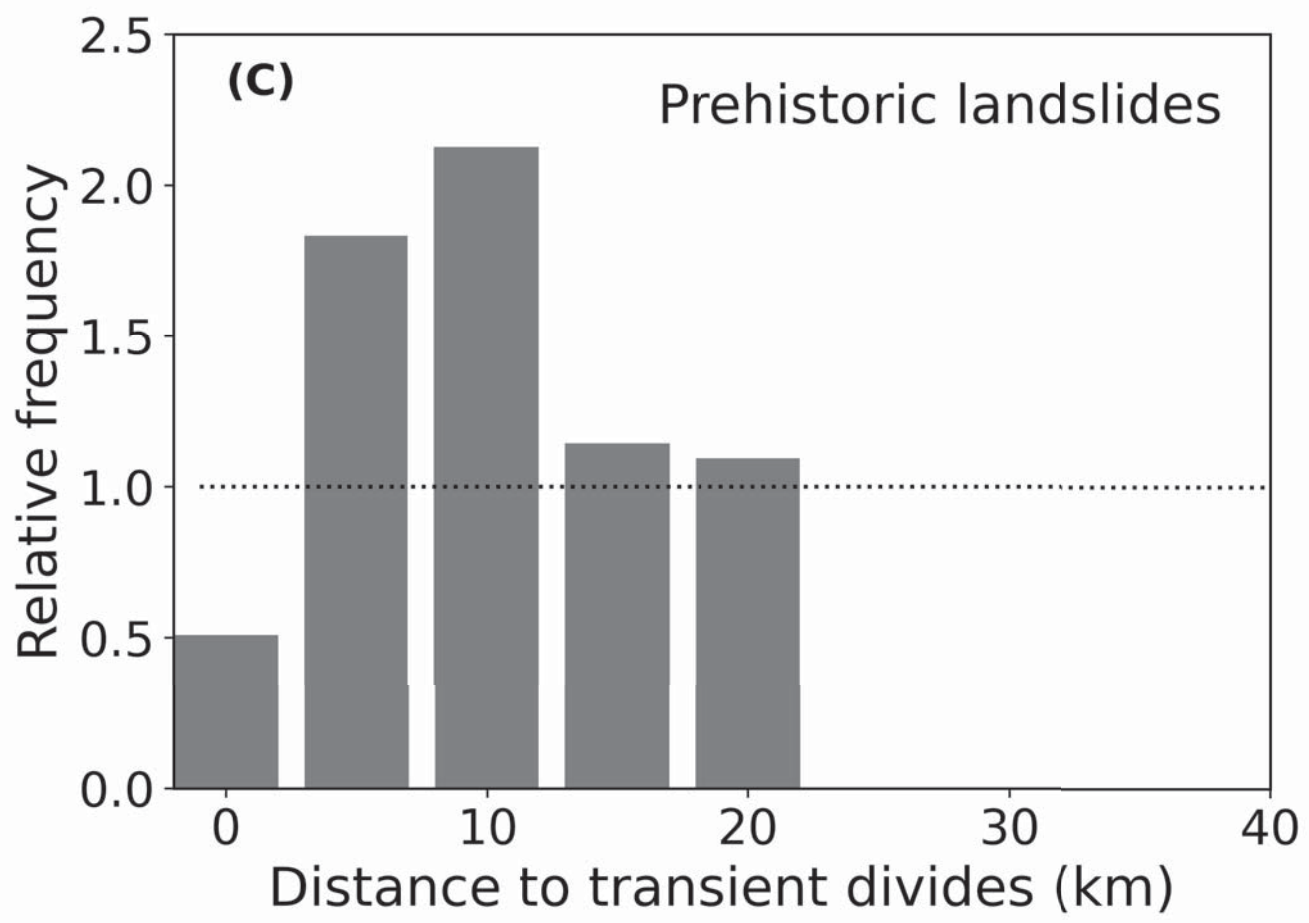


Figure10D.

